A001

Upscaling of Fractured Oil Reservoirs Using Homogenization Including Non-equilibrium Capillary Pressure

H. Salimi* (Delft University of Technology) & J. Bruining (Delft University of Technology)

SUMMARY

Recovery in incompletely water-wet fractured reservoirs can be extremely low. In the laboratory, these systems are often mistaken for oil-wet reservoirs, because imbibition only starts after removal of the oil layer, which originally covers the grains. The long time required to remove the oil film will be referred to as delay time. There are two theories that describe the delay time necessary for removal of an oil film, leading to a capillary pressure that depends on time. One of the theories is developed by Barenblatt et al. and it modifies both the capillary pressure and the relative permeabilities. The other theory is developed by Hassanziadeh et al. and it only deals with the non-equilibrium effect for the capillary pressure.
No attempt has yet been made to model non-equilibrium effects in fractured reservoirs for a field-scale problem and this is an innovative aspect of this paper. To examine whether the non-equilibrium effect has any effect on larger-scale problems, we apply homogenization to derive an upscaled model for fractured reservoirs in which the non-equilibrium effects are included. We formulate a fully implicit three-dimensional upscaled numerical model. Furthermore, we develop a computationally efficient numerical approach to solve the upscaled model. We use the simulation to determine the range of delay times for which discernable effects occur in terms of oil recovery.
It is shown that at low Peclet numbers, i.e., when the residence time of the fluids in the fracture is long with respect to the imbibition time, incorporation of delay times of the order of few months have no significant effect on the oil recovery. However, when the Peclet number is large, the delay times reduce the rate of oil recovery. We will discuss for which values of the delay time (Barenblatt) and capillary-damping coefficient (Hassanizadeh), equivalent results are obtained. This is the first time that such a comparison is made for a field scale project and it shows that both approached show the importance of taking to account delay effects in the capillary pressure behavior.

Introduction

Fractured hydrocarbon reservoirs provide over 20% of the world's oil reserves and production (Saidi 1983; Firoozabadi 2000). Virtually, all reservoirs contain at least some natural fractures (Aguilera 1998; Nelson 2001). However, from the point of view of reservoir modeling, a fractured reservoir is defined as a reservoir in which naturally occurring fractures have a significant effect on fluid flow (Salimi and Bruining 2008, 2009a, 2010a). We only consider reservoirs where fluid flow occurs predominantly in a connected fracture network and do not consider the case of limited connectivity and cases in which fractures act as a barrier for fluid flow. Fractured-reservoir simulations completely differ from conventional-reservoir simulations. The challenge of upscaling is to give an accurate representation of the interaction between fractures and matrix blocks.

Many geological situations lead to some type of fractured reservoirs (Aguilera 1998; Nelson 2001). From the geological point of view, fractured reservoirs can exhibit a number of topologically different configurations. These are reservoirs built from (1) matrix blocks that are bounded by fracture planes in all directions (totally fractured reservoirs, TFRs, or sugar cube), (2) matrix blocks that are bounded only by more or less vertical fracture planes (vertically fractured reservoirs, VFRs), and (3) matrix blocks that form a connected domain interdispersed with fractures (partially fractured reservoirs, PFRs). Matrix blocks in the sugar-cube configuration are pressed against each other, and consequently contact regions are usually crushed and impermeable except in shallow hydrology applications (Dahan et al. 1998; Zanini et al. 2000). It has been argued that the sugar-cube configuration is unrealistic at large depth, because the horizontal fractures will close due to the overburden pressure. This ignores the possibility that two fracture sets are oblique leading to horizontal columns. If these columns are intersected by a third perpendicular fracture set, matrix blocks can occur that are bounded by three fracture planes (Finkbeiner et al. 1997; Teixell et al. 2000). In the VFR configuration, the top and bottom of the columns are bounded by the impermeable cap- and base-rock. From the geological perspective, a VFR is more abundant than a sugar-cube configuration. A VFR cannot be mimicked with a sugar-cube model in which the horizontal fracture is very small because it precludes capillary continuity of stacked matrix blocks. It is also not mimicked by a zero width horizontal fracture because such a fracture will act like a barrier and impedes vertical flow.

The current literature in the petroleum community dealing with flow in fractured reservoirs is largely confined to topological equivalents of the sugar-cube model, i.e., the matrix blocks are surrounded by fractures from all sides (Barenblatt et al. 1960; Warren and Root 1963; Kazemi 1969; Sonier et al. 1988; Kazemi et al. 1992; Al-Huthali and Datta-Gupta 2004; Al-Harbi et al. 2005; Sarma and Aziz 2006). However, the VFR (aggregated-column) model is topologically different because it is not connected to the fracture network through the top and bottom of the matrix column. To our knowledge, the current reservoir simulators have no option to deal with this situation and this is another innovative aspect of this contribution. The novel feature of the upscaled-VFR model is that, for example, fluid may enter the matrix column at one height, travel downward for some time, and then re-enter the fractures at a lower height.

In fractured reservoirs, capillary forces, leading to counter-current or co-current imbibition (Pooladi-Darvish and Firoozabadi 2000; Rangel-German and Kovscek 2002; Behbahani and Blunt 2005; Hatiboglu and Babadagli 2007; Karimaie and Torsæter 2007), are the main drivers for waterdrive recovery from the matrix blocks (Firoozabadi 2000). Reservoir wettability and its effect on oil recovery have been the subject of numerous studies (Tang and Firoozabadi 2001; Anderson 1987; Morrow and Mason 2001; Graue et al. 2001; Seethepalli et al. 2004). However, these studies address drainage and imbibition behavior on a laboratory scale, which describe only one facet of multiphase flow in fractured reservoirs. Therefore, major issues of oil recovery related to wettability at a full-field reservoir scale remain poorly understood (Salimi and Bruining 2010b).

Experimental evidence (Topp et al. 1967; Smiles et al. 1971; Vachaud et al. 1972; Elzeftawy and Mansell 1975; Stauffer 1978; Tang and Firoozabadi 2001; Siemons et al. 2006; Plug and Bruining 2007; Plug et al. 2008; Yu et al. 2009) supports a more general description of capillary pressure and relative permeability functions, which includes a non-equilibrium effect. Reservoir interpretation that

does not recognize the potential for reduced recovery because of non-equilibrium effects may lead to an incorrect estimation of the recovery. The concept of the non-equilibrium effect was first introduced by Barenblatt and his colleagues (Barenblatt 1971; Barenblatt and Gilman 1987; Barenblatt et al. 1997, 2003). It is equivalent to an alternative formulation introduced by Hassanizadeh and Gray (1990, 1993) and Pavone (1990). We follow both the formulation by Barenblatt, which has been worked out for both the capillary-pressure and relative-permeability functions, and the approach by Hassanizadeh, which only includes the capillary pressure. To our knowledge, this problem has not been discussed previously for a field-scale problem and this is another innovative aspect of this study. To examine whether the non-equilibrium effects have any effect on larger-scale problems, we construct an upscaled model in which the non-equilibrium effects are included for the matrix columns. We use the simulation to determine the range of delay times to investigate whether discernable effects occur in terms of oil recovery.

The objective of this paper is (1) the construction of an upscaled model in which the non-equilibrium effect is included; (2) comparison of the Barenblatt's and Hassanizadeh's approach for non-equilibrium capillary pressures in upscaled waterdrive recovery from fractured reservoirs on the field scale; (3) development of an efficient fully implicit numerical method solving the upscaled equations; and (4) quantifying conditions for which non-equilibrium capillary pressure determines the recovery behavior.

The paper is organized as follows. First, we briefly describe the physical model and the topological configuration for vertically fractured reservoirs. Next, we explain the theory of non-equilibrium effects in two-phase flow. Thirdly, we explain the upscaled model. Subsequently, we derive the fully implicit numerical scheme. After that, we introduce the Peclet number to distinguish two different regimes and consider the effect of gravity. Then, we provide numerical simulation at field scale to study the mechanisms mentioned above. Finally, we summarize our findings in the conclusions Section.

Physical Model

In this paper, we extend our previous work (Salimi and Bruining 2009a, 2009b, 2010a) on upscaling waterdrive recovery in fractured reservoirs to include non-equilibrium effect in capillary pressures and relative permeabilities. For reasons of easy reference, we shortly repeat the theory for obtaining the upscaled equations.

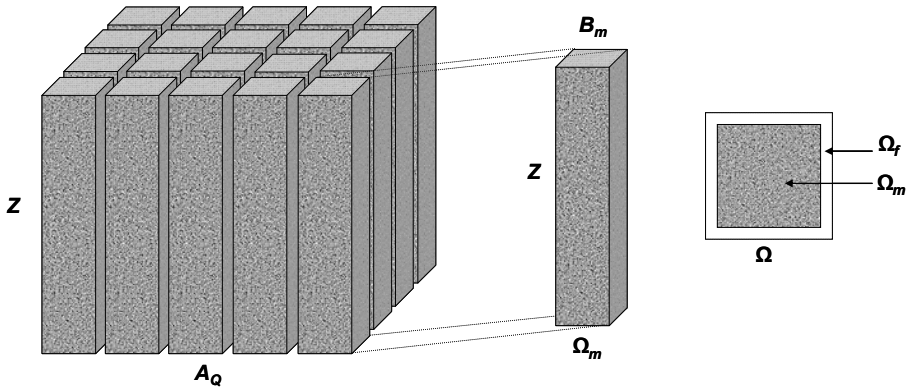

Fig. 1: Vertically fractured network (left), matrix column (middle), and horizontal cross section (right) of a small unit that consists of a matrix part and fracture part.

We consider a vertically fractured network (Fig. 1) in the domain $Q = A_Q \times Z$, where $A_Q = \{x, y \in \mathrm{R} |\ 0 \le x \le L,\ 0 \le y \le W\}$ and $Z = \{z \in \mathrm{R} |\ 0 \le z \le H\}$, where R represents the set of real numbers. We use L, W, and H to denote the length, width and height of the fractured reservoir. There are two mutually perpendicular vertical fracture sets F_1, F_2, which surround the matrix column $B_m = \Omega_m \times Z$, where Ω_m (see Fig. 1) denotes the domain of a horizontal cross-section of a matrix column. Therefore, matrix columns are connected from the top to the bottom of the reservoir domain and there is no direct horizontal fracture connection between matrix columns. Thus, the matrix

columns can capture phase segregation caused by gravity. Half of the fracture space surrounding the matrix columns occupy the domain $B_f = \Omega_f \times Z$. Furthermore, $B = \Omega \times Z$ denotes the small periodic units that occupy the domain $B = B_f \cup B_m$. All the small units together constitute the VFR.

We simulate the injection of water into a vertically fractured oil reservoir. We apply continuity of capillary pressure and continuity of fluid flow as boundary conditions on the vertical interfaces between fracture and matrix columns. Flux continuity follows from fluid conservation at the interface between fracture and matrix. There is capillary pressure continuity at the boundary of fractures and matrix columns unless one of the phases either in the matrix or in fracture is immobile (Van Duijn et al. 1995). Indeed when one of the phases is immobile, the pressure of that phase depends on local conditions and cannot be determined globally. Hence, the capillary pressure, which is the difference between the phase pressure of the non-wetting phase and wetting phase, can be discontinuous. However, as residual saturations do not flow, this presents no difficulties for the modeling. Continuity of force, and hence continuity of phase pressures, implies continuity of capillary pressure when both phases are mobile.

Moreover, we incorporate the gravity effect directly inside the matrix columns. As a result, there is a net flow within the matrix columns. The symmetry of the fracture pattern in the horizontal plane is such that the fracture permeability can be considered isotropic. We only consider two-phase (oil and water) incompressible flow where the water viscosity, μ_w, and the oil viscosity, μ_o, are assumed to be constant.

Model Equations

We use the two-phase ($\alpha = o, w$) extension of Darcy's law for constant fluid densities

$$\begin{aligned}\mathbf{u}^*_{\alpha f} &= -\frac{k^*_f k_{r\alpha,f}}{\mu_{\alpha f}} \nabla\left(P_{\alpha f} + \rho_\alpha g z\right) := -\lambda^*_{\alpha f} \nabla \Phi_{\alpha f}, \\ \mathbf{u}_{\alpha m} &= -\frac{k_m k_{r\alpha,m}}{\mu_{\alpha m}} \nabla \Phi_{\alpha m} := -\lambda_{\alpha m} \nabla \Phi_{\alpha m}.\end{aligned} \tag{1}$$

In these equations the superscript (*) denotes the intrinsic (local) fracture properties. The intrinsic fracture permeability evaluated inside the fracture is denoted by k_f^*. We define the intrinsic fracture permeability k_f^* based on the fracture aperture. The matrix permeability is denoted by k_m. Relative permeabilities are denoted by $k_{rw,\zeta}$ and $k_{ro,\zeta}$, where $\zeta = f, m$ indicates the fracture or matrix systems. Here P is the pressure, ρ is the fluid density, g is the gravity acceleration factor and z is the vertical upward direction. We define a phase mobility $\lambda_\alpha = k \times k_{r\alpha}/\mu_\alpha$ as the ratio between the phase permeability and fluid viscosity. The phase potential Φ_α is equal to the pressure plus the gravity term.

The mass conservation equation reads

$$\frac{\partial}{\partial t}\left(\varphi_\zeta \rho_{\alpha\zeta} S_{\alpha\zeta}\right) + \nabla \cdot \left(\mathbf{u}_{\alpha\zeta} \rho_{\alpha\zeta}\right) = 0, \tag{2}$$

where φ is the porosity and S_α is the phase saturation. We obtain the governing equations describing incompressible two-phase flow by combining Darcy's Law (Eq. 1) and the mass conversation (Eq. 2)

$$\frac{\partial}{\partial t}\left(\varphi^*_f \rho_{\alpha f} S_{\alpha f}\right) = \nabla \cdot \left(\rho_{\alpha f} \lambda^*_{\alpha f} \nabla \Phi_{\alpha f}\right) \text{ in } \Omega_f, \tag{3}$$

$$\frac{\partial}{\partial t}\left(\varphi_m \rho_{\alpha m} S_{\alpha m}\right) = \nabla \cdot \left(\rho_{\alpha m} \lambda_{\alpha m} \nabla \Phi_{\alpha m}\right) \text{ in } \Omega_m. \tag{4}$$

We define a capillary pressure $P_c = P_o - P_w$. This capillary pressure is at equilibrium. At the interface between the fracture and matrix systems, there is continuity of water and oil flow

$$\left(\rho_{\alpha f} \lambda^*_{\alpha f} \nabla \Phi_{\alpha f}\right) \cdot \mathbf{n} = \left(\rho_{\alpha m} \lambda_{\alpha m} \nabla \Phi_{\alpha m}\right) \cdot \mathbf{n} \quad \text{on } \partial\Omega_m, \tag{5}$$

where **n** denotes the outward unit normal vector to the surface ($\partial\Omega_m$) pointing from the matrix to the fracture. At the interface, there is also continuity of capillary pressure (Van Duijn et al. 1995). Whenever the capillary-pressure function (curve) would be different for two media that are connected with an interface, continuity of capillary pressure results in a discontinuity in saturation. That is the case for fracture-matrix interface since the fracture capillary pressure is smaller than the matrix capillary pressure due to the huge contrast between the intrinsic fracture and matrix permeability. For matrix blocks that are connected to more than one fracture, there is more than one fracture-matrix interface. Consequently, each fracture-matrix interface has its own state of continuity of capillary pressure. If matrix blocks have different flow functions (i.e., capillary-pressure function), continuity of capillary pressure leads to different discontinuities of saturation for each matrix block accordingly (Salimi and Bruining 2010a).

Non-Equilibrium Effects

The classical two-phase flow model proposed by Muskat and Meres (1936), and Leverett (1939) is based upon the fundamental assumption that the local state of the flow is in equilibrium. This means that the two-phase functions k_{rw}, k_{ro}, and Leverett J-function are only functions of the water saturation S_w, independent of whether the water saturation decreases or increases. Therefore, at local equilibrium we have

$$k_{rw} = k_{rw}(S_w), \qquad k_{ro} = k_{ro}(S_w), \qquad P_c(S_w) = \sigma_{wo}\sqrt{\frac{\varphi}{k}}J(S_w), \tag{6}$$

where σ_{wo} is the oil-water interfacial surface tension coefficient, and φ and k are, respectively, the porosity and the absolute permeability of the rock. The dimensionless Leverett J-function is often assumed to be independent of the porosity and permeability for a specific litho-type.

For increasing (wetting) water saturation, the wetting phase will flow initially in the larger pores, but when steady state ($\partial S_w/\partial t = 0$) is attained it withdraws in the narrower pores and corners and Eq. 6 becomes applicable. There are two reasons that water flows in the larger pores. First, the "permeability" of a cylindrical pore is proportional to the square of the pore radius R, whereas the capillary driving force is inversely proportional to R. Hence, even if capillary forces are smaller in bigger pores the velocity is still larger due to the higher permeability. The other reason is that the pores that were originally filled with oil will maintain an oil film at the wall, which is only slowly removed. In other words, a water-wet medium will effectively be oil-wet in the early stages of imbibition. The slow removal rate of an oil film shows itself in experiments on contact angle measurements. For water-wet media with a finite contact angle, it is possible that the delay time is a few months. This effect is observed in many spontaneous imbibition experiments (Topp et al. 1967; Smiles et al. 1971; Vachaud et al. 1972; Elzeftawy and Mansell 1975; Stauffer 1978; Tang and Firoozabadi 2001; Siemons et al. 2006; Plug and Bruining 2007; Plug et al. 2008; Yu et al. 2009). During the transition, the wetting fluid relative permeability is higher than in steady state conditions. Similarly, during the redistribution of the flow paths both the relative permeability of the non-wetting fluid and the capillary pressure are lower than in steady-state flow. Strictly speaking, this reasoning implies that the relative permeability and capillary pressure functions obtained in steady-state flow experiments cannot be used in transient processes whose characteristic transition times are comparable with characteristic fluid redistribution times. However, due to the monotonous behavior of these functions, (see Fig. 2), they can still be used to characterize transient flow by evaluating the functions at some effective water saturations. Indeed, the relative permeabilities and the capillary pressure are evaluated not at the actual instantaneous values of the saturation S_w, but at some effective saturation $\eta \geq S_w$, see Fig. 2. The effective saturation η is always larger than the water saturation S_w or equal to it when steady state is attained. The concept of effective saturation was first introduced by Barenblatt and his colleagues (Barenblatt 1971; Barenblatt and Gilman 1987; Barenblatt et al. 1997, 2003). It is equivalent to an alternative formulation introduced by Hassanizadeh and Gray (1993) (see also Hassanizadeh et al. 2002).

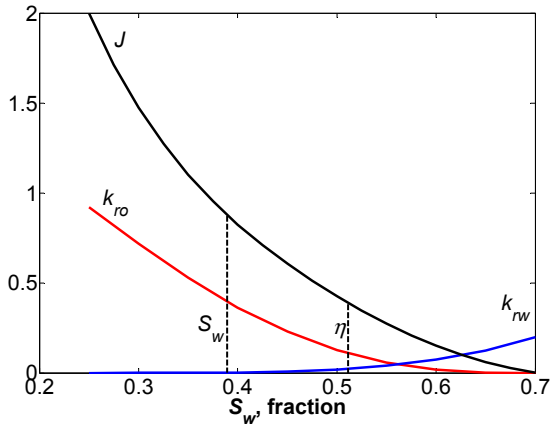

Fig. 2: The effective saturation η is always higher than the actual water saturation S_w.

In general, the effective saturation η can be different for both the relative permeability curves ($k_{r\alpha}$) and the Leveret J-function (J). However, following Barenblatt (1971), Barenblatt and Gilman (1987), and Barenblatt et al. (2003), we assume that the effective saturation is the same for all three functions. Thus, instead of the relationships in Eq. 6 we have

$$k_{rw} = k_{rw}(\eta), \qquad k_{ro} = k_{ro}(\eta), \qquad P_c(\eta) = \sigma_{wo}\sqrt{\frac{\varphi}{k}}\,J(\eta), \tag{7}$$

where the functions k_{rw}, k_{ro}, and J are the same functions as in Eq. 6.

Due to the non-equilibrium effects, the relationship between η and S_w must be a time-dependent function. We use the hypothesis (Barenblatt 1971; Barenblatt et al. 1997, 2003) that there is a relationship between the local effective water saturation η and the actual water saturation S_w and its rate of change $\partial S_w/\partial t$. Dimensional analysis suggests that such a relationship must include a characteristic redistribution time. Further, linearization of this relationship yields

$$\tau_b \frac{\partial S_w}{\partial t} = \eta - S_w. \tag{8}$$

Here, τ_b is a coefficient having the dimension of time. If the effective water saturation η were fixed and τ_b were constant, then the difference $(\eta - S)$ would decay exponentially as $\exp(-t/\tau_b)$. Therefore, τ_b is a characteristic relaxation time (delay time) needed for the rearrangement of the menisci and flow paths to a new steady state configuration. Note that in spontaneous imbibition such a steady state is never achieved. Indeed, the redistribution time, τ_b, may depend on the saturation, but we assume that τ_b is constant.

Hassanizadeh and Gray (1990, 1993) derived an alternative theory to deal with non-equilibrium effects based on non-equilibrium thermodynamics. The main constitutive hypothesis in their theory is the dependence of the Helmholtz free energy functions for the phases and interfaces on state variables such as mass density, temperature, saturation, porosity, interfacial area, and the solid phase strain tensor. Explicit inclusion of interfaces and interfacial properties in the macroscale theory of the two-phase flow is an essential characteristic of Hassanizadeh's theory. In this approach, the macroscopic capillary pressure is defined solely as an intrinsic property of the system and is not simply equal to the difference in fluid-phase pressures. They have proposed that the difference in fluid pressures may not only depend on saturation, but also on the rate of change of saturation. Their result using a linear approximation is

$$P_c^{dyn} - P_c^{stat} = \tau_h \frac{\partial S_o}{\partial t}, \tag{9}$$

where P_c^{dyn} denotes the difference between nonwetting-phase pressure (P_n) and wetting-phase pressure (P_w), which is the commonly measured quantity. P_c^{stat} denotes the equilibrium (or "static") capillary pressure, and τ_h is a capillary-damping coefficient that may still depend on saturation. Note

that τ_h is non-negative, because heat dissipation is always positive. Eq. 9 suggests that at a given point in the system and at any given time, saturation will change locally in order to restore equilibrium; that is at equilibrium there is equivalence between (P_n – P_w) and P_c^{stat}. If τ_h is found to be small, equivalence between P_c^{dyn} and P_c^{stat} will be re-established instantaneously after equilibrium is disturbed. For porous media with high permeability, the non-equilibrium effect is less pronounced. As permeability decreases, the applicability of the non-equilibrium concept becomes more pronounced.

The non-equilibrium theory of capillary pressure of Hassanizadeh and Gray versus Barenblatt cannot be related if constant values of τ_b and τ_h are used. Hassanizadeh and Gray (1990, 1993) do not deal with relative permeabilities, but their theory is based on fundamental non-equilibrium thermodynamic principles, whereas the theory of Barenblatt et al. (1997, 2003) is based on insight that initially larger pores will be filled with water before the water withdraws into the smaller pores after removal of the oil film covering the pores. If we would have a linear saturation dependence of the capillary pressure, e.g.,

$$P_c^{stat} = P_c^{\circ} + \Lambda\left(1 - S_{or} - S_w\right), \tag{10}$$

we can relate the delay time τ_b to the capillary-damping coefficient τ_h as

$$\Lambda \tau_b = \tau_h, \tag{11}$$

where Λ is a constant coefficient. In spite of the fact that the capillary pressure is a nonlinear function of the saturation, we still use this as a basis for comparisons. For non-linear capillary pressure, we can approximate the capillary pressure by using the average capillary derivative for calculating Λ.

To the best of our knowledge, no attempt has yet been made to model non-equilibrium effects in fractured reservoirs by scaling. In this work, we only consider the non-equilibrium effect for the matrix columns because the important process, i.e., capillary imbibition, occurs in the matrix columns and because the matrix system has a low permeability with respect to the fracture system. The system of Eqs. 7 and 8 for Barenblatt's approach and Eq. 9 for Hassanizadeh's approach can be straightforwardly implemented in Eqs. 4 and 5 and constitute the basic mathematical model for our further consideration of the non-equilibrium two-phase flows in VFRs.

Upscaled Model

The previously derived upscaled equations (Salimi and Bruining 2009a) in the VFR with homogenization are

$$\frac{\partial}{\partial t}\left(\varphi_f S_{wf}\right) - \nabla_b \cdot \left(\lambda_{wf} \nabla_b \Phi_{wf}\right) + \frac{1}{|\Omega|}\int_{\Omega_m}\left\{\frac{\partial}{\partial t}\left(\varphi_m S_{wm}\right) - \frac{\partial}{\partial z}\left(\lambda_{wm}\frac{\partial}{\partial z}\Phi_{wm}\right)\right\}\mathrm{d}\mathbf{x}_s = q_{ext,w} \quad \text{in } Q, \tag{12}$$

$$\begin{aligned} &-\nabla_b \cdot \left(\left(\lambda_{wf} + \lambda_{of}\right)\nabla_b \Phi_{wf} + \lambda_{of}\nabla_b \Phi_{cf}\right) + \\ &\quad + \frac{1}{|\Omega|}\int_{\Omega_m}\left\{-\frac{\partial}{\partial z}\left(\left(\lambda_{wm} + \lambda_{om}\right)\frac{\partial}{\partial z}\Phi_{wm} + \lambda_{om}\frac{\partial}{\partial z}\Phi_{cm}\right)\right\}\mathrm{d}\mathbf{x}_s = q_{ext,w} + q_{ext,o} \quad \text{in } Q, \end{aligned} \tag{13}$$

where $q_{ext,w}$ and $q_{ext,o}$ are the external flow rates that come from the production and injection wells. The phase potential Φ_α is equal to the pressure (P) plus the gravity term. Here, we also define the capillary potential $\Phi_c = P_c + (\rho_o - \rho_w)gz$. The integral term is the exchange term of fluid flow at the interface between the fracture and matrix. Here, the global fracture porosity and (effective) permeability are given as

$$\varphi_f = \frac{1}{|\Omega|}\int_{\Omega_f}\varphi_f^* \mathrm{d}\mathbf{x}_s, \tag{14}$$

$$k_f = \frac{1}{|\Omega|}\int_{\Omega_f} k_f^*\left(\mathrm{I} + \nabla_s \otimes \left(\omega_1, \omega_2, 0\right)\right)\mathrm{d}\mathbf{x}_s. \tag{15}$$

We use φ_f^* to denote the intrinsic fracture porosity, and $|\Omega|$ to denote the combined fracture and matrix domain. The integration is over the local domain, which is a small unit cell that contains a specific matrix-column size and fracture aperture for the grid cell. In the same way, we use k_f^* to denote the intrinsic fracture permeability. The behavior of ω_1 (ω_2) is a measure of the potential fluctuation caused by the non-homogeneous nature of the fractured reservoir that is subjected to a global potential gradient in the x-direction (y-direction). The VFR does not need an upscaling procedure in the z-direction, which is a reason that we only consider the vector (ω_1, ω_2, 0). The cell equation required to solve for (ω_1, ω_2, 0) can be found in Salimi and Bruining (2009a).

To include the non-equilibrium effects in the upscaled model, we couple Eqs. 7 and 8 for Barenblatt's and Eq. 9 for Hassanizadeh's approach to the matrix-column equations. The equations for the matrix columns using Barenblatt's approach are

$$\frac{\partial}{\partial t}\left(\varphi_m S_{wm}\right) - \nabla_s \cdot \left(\lambda_{wm}(\eta)\nabla_s \Phi_{wm}\right) = 0 \quad \text{in } B_m, \tag{16}$$

$$-\nabla_s \cdot \left(\left(\lambda_{wm}(\eta) + \lambda_{om}(\eta)\right)\nabla_s \Phi_{wm} + \lambda_{om}\nabla_s \Phi_{cm}(\eta)\right) = 0 \quad \text{in } B_m, \tag{17}$$

and Eq. 8. At the interface between the fracture and matrix systems, there are continuity of water and oil flow and continuity of capillary pressure. The boundary conditions on the vertical faces of the matrix columns read

$$\Phi_{wm}\left(t, x_b, x_s\right) = \Phi_{wf}\left(t, x_b\right), \quad \text{and} \quad \Phi_{cm}\left(t, x_b, x_s, \eta\right) = \Phi_{cf}\left(t, x_b\right), \tag{18}$$

where x_b denotes the global scale and x_s denotes the local scale. Our choice for the small-unit scale is a single matrix column of which vertical faces are surrounded by fractures and its horizontal faces (e.g., top and bottom) are connected to the cap and base rock. We define the global scale as the dimension of the grid-block scale.

For the non-equilibrium theory by Hassanizadeh et al., the phase mobility λ_α in Eqs. 16 and 17 is now a function of water saturation S_w instead of the effective water saturation η, and the matrix capillary potential Φ_{cm} in Eqs. 17 and 18 is replaced by Φ_{cm}^{dyn}. Moreover, Eq. 10 is coupled to the matrix equation to relate the dynamic (non-equilibrium) capillary pressure to the static (equilibrium) capillary pressure.

There are no-flow boundary conditions on the top and bottom of the entire fractured reservoir, i.e.,

$$-\lambda_{\alpha\zeta}\nabla\Phi_{\alpha\zeta}.\mathbf{n} = 0, \quad \alpha = w, o, \quad \text{and} \quad \zeta = f, m, \tag{19}$$

where $\mathbf{n}$ denotes the outward unit normal vector to the surface.

The derivation of the upscaled model including the non-equilibrium effects is complete. To our knowledge, there exist no analytical nor numerical results for the upscaled-VFR model described above. In the next Section, we develop an efficient numerical method to solve the complex system of equations in a vertically fractured reservoir.

Numerical Solution

The numerical procedure described below is an extension of the method used by Arbogast (1997) and Salimi and Bruining (2010a) for the sugar-cube model. The difficulty arises due to a coupling of flow in the vertical direction, which is important in the upscaled-VFR model. From the computational point of view, we consider a matrix column associated with each point in the base plane of the reservoir. The horizontal cross-sectional position of any point $\mathbf{r}_b = (x_b, y_b, z_b) \in Q$, is denoted by $\mathbf{r'}_b = (x_b, y_b) \in A_Q$. The matrix column at $\mathbf{r'}_b = (x_b, y_b) \in A_Q$ is denoted by $B_m(\mathbf{r'}_b) = \Omega_m(\mathbf{r'}_b) \times H$, where this matrix column is representative of matrix columns in the vicinity of $\mathbf{r'}$. We formulate our numerical method in terms of the water potential, the capillary pressure, and the water saturation. Here, we also define the capillary potential $\Phi_c = P_c + (\rho_o - \rho_w)gz$. We assume that all external sources, i.e., the production and injection wells, influence only the fractures. Eqs. 12 and 16 below are called

the saturation equations, and the sums over the phases of each of the two-phase equations are Eqs. 13 and 17, the pressure equations.

Initially, there is capillary-gravity equilibrium both in the fracture system and in the matrix column. This means that the fluid-exchange term between fracture and matrix is zero initially. In addition, the effective water saturation η is equal to the actual water saturation S_w for Barenblatt's approach, and the dynamic capillary potential Φ_{cm}^{dyn} is the same as the static (equilibrium) capillary potential Φ_{cm}^{stat} for Hassanizadeh's approach. Since initial oil-in-place is known, we determine the initial fracture water potential by solving the fracture pressure equation (Eq. 13). Because of equilibrium, we can solve the matrix pressure equation (Eq. 17) to obtain the initial matrix water potential.

Equations 8, 9, and 12 through 19 cannot be solved sequentially or explicitly, because a small change in the boundary values on each matrix column can cause flow of a volume of fluid that is large in comparison to the volume of the fractures (Douglas et al. 1991). In other words, the matrix absorbs more fluid from the surrounding fractures in one step than can be resident there. Part of the excess volume in the matrix is returned to the fractures in the next step, however, violating mass conservation. Therefore, the fracture-matrix interaction must be handled implicitly.

We use a backward-Euler time approximation for the complete system of Eqs. 8, 9, and 12 through 19. We further use a finite-volume approach and first-order upwind scheme for spatial discretization. To facilitate the implementation of the no-flow boundary conditions and the continuity conditions of the potentials along the fracture-matrix interfaces, we discretize the space variables in a cell-centered manner in the fractures and also cell-centered with respect to z in the matrix columns. However, the discretization in the x_s and y_s are vertex-centered. In this work, we use uniform grid cells in the fractures and in each matrix column. From the computational perspective, we consider a case in which the vertical discretization in the matrix columns coincides with that in the fractures.

We discretize Q into $N_{xf} \times N_{yf} \times N_{zf}$ grid cells, each grid cell of size $d_{xf} \times d_{yf} \times d_{zf}$. The center of the fracture-cell $\mathbf{p} = (p_x, p_y, p_z)$ is then

$$\mathbf{x}_{bp} = \left((p_x - 1/2)d_{xf}, (p_y - 1/2)d_{yf}, (p_z - 1/2)d_{zf}\right),$$

and the set of all fracture grid cell centers is

$$N_f = \left\{x_{bp_i} : p_i = 1,2,3,..., N_{if}, i = x, y, z\right\}.$$

This reduces the system of the equations to a fully discrete, three-dimensional problem. We denote the vectors of unknowns in the fracture by

$$\vec{\Phi}_{wf}^{n} = \left\{\Phi_{wf,i}^{n}, i = 1,2,3,..., N_{xf} \times N_{yf} \times N_{zf}\right\},$$
$$\vec{S}_{wf}^{n} = \left\{S_{wf,i}^{n}, i = 1,2,3,..., N_{xf} \times N_{yf} \times N_{zf}\right\},$$

where superscript n denotes the time level n. In the vector, the potentials and saturations are stacked behind each other. At each $\mathbf{x}_{bp} \in N_f$, there is a representative matrix column $B_m(\mathbf{x}_{bp'}) = (0, d_{xm} N_{xm}) \times (0, d_{ym} N_{ym}) \times (0, d_{zf} N_{zf})$, where $\mathbf{p}' = (p_x, p_y)$ is the projection of $\mathbf{p}$ on the x-y plane. Then, the center point of each matrix cell $\mathbf{c} = (c_x, c_y, c_z)$ is

$$\mathbf{x}_{sp'} = (c_x d_{xm,p'}, c_y d_{ym,p'}, (c_z - 1/2)d_{xf}),$$

and the set of all matrix-cell-center points at fracture point $\mathbf{p}$ is given by

$$N_{m,p'} = \left\{x_{sp',c_i} : c_i = 0,1,..., N_{im,p'}, i = x, y; c_z = 1,2,..., N_{zf}\right\}.$$

Then, associated with each grid point $i = 1, 2, \ldots, N_{xf} \times N_{yf} \times N_{zf}$, we have three series of matrix unknowns

$$\vec{\Phi}_{wm,i'}^{n} = \left\{\Phi_{wm,i'j}^{n}, i' = 1,2,..., N_{xf} \times N_{yf}, j = 1,2,3,..., N_{xm} \times N_{ym} \times N_{zf}\right\},$$

$$\vec{S}^{n}_{wm,i'} = \left\{ S^{n}_{wm,i'j}, i' = 1,2,...,N_{xf} \times N_{yf}, j = 1,2,3,...,N_{xm} \times N_{ym} \times N_{zf} \right\},$$
$$\vec{\eta}^{n}_{wm,i'} = \left\{ \eta^{n}_{wm,i'j}, i' = 1,2,...,N_{xf} \times N_{yf}, j = 1,2,3,...,N_{xm} \times N_{ym} \times N_{zf} \right\},$$

in the m^{th} matrix column. For Hassanizadeh's approach, the unknown vector of the effective water saturation is replaced by an unknown vector of the dynamic capillary potential Φ_{cm}^{dyn}. After that, we can write the fully discrete, nonlinear fracture and matrix equations

$$\begin{cases} F_i\left(\vec{\Phi}^{n}_{wf}, \vec{S}^{n}_{wf}, \vec{\Phi}^{n}_{wm}, \vec{S}^{n}_{wm}\right) = 0, & i = 1,2,...,N_{xf} \times N_{yf} \times N_{zf}, \\ M_{i'j}\left(\vec{\Phi}^{n}_{wf}, \vec{S}^{n}_{wf}, \vec{\Phi}^{n}_{wm,i'}, \vec{S}^{n}_{wm,i'}, \vec{\eta}^{n}_{wm,i'}\right) = 0, & \begin{cases} i' = 1,2,...,N_{xf} \times N_{yf}, \\ j = 1,2,...,N_{xm} \times N_{ym} \times N_{zf}, \end{cases} \end{cases} \tag{20}$$

where F_i and $M_{i'j}$ are some nonlinear functions. Again, the effective water saturation in function M is replaced by the dynamic capillary potential for Hassanizadeh's approach. We use Newton's method to linearize the above system of equations. Let

$\vec{\Phi}^{n,k}_{wf}$, $\vec{S}^{n,k}_{wf}$, $\vec{\Phi}^{n,k}_{wm}$, $\vec{S}^{n,k}_{wm}$ and $\vec{\eta}^{n,k}_{wm}$,

denote the k^{th} Newton iteration for the n^{th} time level's solution. We write the evaluation of F and M at the $(k\text{-}1)^{th}$ iteration for the n^{th} time level solution as

$$\begin{cases} F_i^{n,k-1} = F_i\left(\vec{\Phi}^{n,k-1}_{wf}, \vec{S}^{n,k-1}_{wf}, \vec{\Phi}^{n,k-1}_{wm}, \vec{S}^{n,k-1}_{wm}\right), \\ M_{i'j}^{n,k-1} = M_{i'j}\left(\vec{\Phi}^{n,k-1}_{wf}, \vec{S}^{n,k-1}_{wf}, \vec{\Phi}^{n,k-1}_{wm,i'}, \vec{S}^{n,k-1}_{wm,i'}, \vec{\eta}^{n,k-1}_{wm,i'}\right). \end{cases}$$

Let ∂_π denote the partial derivative with respect to π. We will develop an efficient numerical scheme based on the conventional Newton procedure. Such a conventional procedure would run as follows:

(1) Start with an initial guess for the solution

$\vec{\Phi}^{n,0}_{wf}$, $\vec{S}^{n,0}_{wf}$, $\vec{\Phi}^{n,0}_{wm}$, $\vec{S}^{n,0}_{wm}$, and $\vec{\eta}^{n,0}_{wm}$.

Note that we use the initial water potential and water saturation as a first guess for the Newton iteration of the first time step. The initial capillary potentials Φ_c in the fracture system and in the matrix column should agree on the matrix column boundary, i.e., continuity of capillary pressure. For non-equilibrium theory by Hassanizadeh, continuity of capillary pressure is between the fracture capillary potential and the matrix dynamic capillary potential (Φ_{cm}^{dyn}) instead of the static capillary potential.

(2) For each k = 1, 2, …, n until convergence is reached:

(a) Solve for

$\vec{\Phi}^{n,k}_{wf}$, $\vec{S}^{n,k}_{wf}$, $\vec{\Phi}^{n,k}_{wm}$, $\vec{S}^{n,k}_{wm}$, and $\vec{\eta}^{n,k}_{wm}$,

satisfying

$$\begin{cases} F_i^{n,k-1} + \sum_{i''=1}^{N_f} \left\{ \left[\partial_{\Phi_{wf,i''}} F_i^{n,k-1} \delta\Phi^{n,k}_{wf,i''} + \partial_{S_{wf,i''}} F_i^{n,k-1} \delta S^{n,k}_{wf,i''} \right] + \right. \\ \left. + \sum_{j'=1}^{N_m} \left[\partial_{\Phi_{wm,i''j'}} F_i^{n,k-1} \delta\Phi^{n,k}_{wm,i''j'} + \partial_{S_{wm,i''j'}} F_i^{n,k-1} \delta S^{n,k}_{wm,i''j'} + \partial_{\eta_{wm,i''j'}} F_i^{n,k-1} \delta\eta^{n,k}_{wm,i''j'} \right] \right\} = 0, \quad i = 1,2,...,N_f, \\ M_{i'j}^{n,k-1} + \sum_{l=1}^{N_{zf}} \left[\partial_{\Phi_{wf,(i',l)}} M_{i'j}^{n,k-1} \delta\Phi^{n,k}_{wf,(i',l)} + \partial_{S_{wf,(i',l)}} M_{i'j}^{n,k-1} \delta S^{n,k}_{wf,(i',l)} \right] + \quad \begin{cases} i' = 1,2,...,N_{xf} \times N_{yf}, \\ j = 1,2,...,N_m. \end{cases} \\ + \sum_{j'=1}^{N_m} \left[\partial_{\Phi_{wm,i'j'}} M_{i'j}^{n,k-1} \delta\Phi^{n,k}_{wm,i'j'} + \partial_{S_{wm,i'j'}} M_{i'j}^{n,k-1} \delta S^{n,k}_{wm,i'j'} + \partial_{\eta_{wm,i'j'}} M_{i'j}^{n,k-1} \delta\eta^{n,k}_{wm,i'j'} \right] = 0, \end{cases} \tag{21}$$

(b) Update the potential and saturations

$$\vec{\Phi}_{wf}^{n,k} = \vec{\Phi}_{wf}^{n,k-1} + \delta\vec{\Phi}_{wf}^{n,k}, \quad \vec{S}_{wf}^{n,k} = \vec{S}_{wf}^{n,k-1} + \delta\vec{S}_{wf}^{n,k},$$
$$\vec{\Phi}_{wm}^{n,k} = \vec{\Phi}_{wm}^{n,k-1} + \delta\vec{\Phi}_{wm}^{n,k}, \quad \vec{S}_{wm}^{n,k} = \vec{S}_{wm}^{n,k-1} + \delta\vec{S}_{wm}^{n,k}, \quad \vec{\eta}_{wm}^{n,k} = \vec{\eta}_{wm}^{n,k-1} + \delta\vec{\eta}_{wm}^{n,k}.$$

This would complete the algorithm for a time step. The above linear system (Eq. 21) involves the solution of a $(2\times N_f + 3\times N_{xf}\times N_{yf}\times N_m) \times (2\times N_f + 3\times N_{xf}\times N_{yf}\times N_m)$ matrix for each Newton iteration at a time step, which is computationally expensive. Within the linearized Newton problem (Eq. 21), the matrix solutions in the i'^{th} column depend on $\Phi_{wf,(i',l)}^{n,k}$ and $S_{wf,(i',l)}^{n,k}$, where l =1, 2, …, N_{zf}. In other words, the matrix solution in the i'^{th} column only depends on all the fracture cells surrounding the matrix column of interest. It is therefore possible to develop an efficient numerical scheme by decoupling the matrix and fracture problems without affecting the implicit nature of the scheme. We replace the matrix problem in Eq. 21 by the following three types of problems for

$$\left(\tilde{\delta}\vec{\Phi}_{wm,(i',l)}^{n,m}, \tilde{\delta}\vec{S}_{wm,(i',l)}^{n,m}, \tilde{\delta}\vec{\eta}_{wm,(i',l)}^{n,m}\right), \quad \left(\hat{\delta}\vec{\Phi}_{wm,(i',l)}^{n,m}, \hat{\delta}\vec{S}_{wm,(i',l)}^{n,m}, \tilde{\delta}\vec{\eta}_{wm,(i',l)}^{n,m}\right), \quad \text{and} \quad \left(\bar{\delta}\vec{\Phi}_{wm,i'}^{n,m}, \bar{\delta}\vec{S}_{wm,i'}^{n,m}, \tilde{\delta}\vec{\eta}_{wm,i'}^{n,m}\right),$$

where $\tilde{\delta}$'s, $\hat{\delta}$'s, and $\bar{\delta}$'s satisfy three types of problems as follows:

Firstly, for each i' = 1, 2, …, $N_{xf}\times N_{yf}$ and j = 1, 2, 3,…, N_m,

$$M_{i'j}^{n,k-1} + \sum_{j'=1}^{N_m}\left[\partial_{\Phi_{wm,i'j'}} M_{i'j}^{n,k-1}\bar{\delta}\Phi_{wm,i'j'}^{n,k} + \partial_{S_{wm,i'j'}} M_{i'j}^{n,k-1}\bar{\delta}S_{wm,i'j'}^{n,k} + \partial_{\eta_{wm,i'j'}} M_{i'j}^{n,k-1}\bar{\delta}\eta_{wm,i'j'}^{n,k}\right] = 0, \tag{22}$$

secondly, for l = 1, 2, …, N_{zf},

$$\partial_{\Phi_{wf,(i',l)}} M_{i'j}^{n,k-1} + \\ + \sum_{j'=1}^{N_m}\left[\partial_{\Phi_{wm,i'j'}} M_{i'j}^{n,k-1}\tilde{\delta}\Phi_{wm,(i',l),j'}^{n,k} + \partial_{S_{wm,i'j'}} M_{i'j}^{n,k-1}\tilde{\delta}S_{wm,(i',l),j'}^{n,k} + \partial_{\eta_{wm,i'j'}} M_{i'j}^{n,k-1}\tilde{\delta}\eta_{wm,(i',l),j'}^{n,k}\right] = 0, \tag{23}$$

thirdly, for l = 1, 2, …, N_{zf},

$$\partial_{S_{wf,(i',l)}} M_{i'j}^{n,k-1} + \\ + \sum_{j'=1}^{N_m}\left[\partial_{\Phi_{wm,i'j'}} M_{i'j}^{n,k-1}\hat{\delta}\Phi_{wm,(i',l),j'}^{n,k} + \partial_{S_{wm,i'j'}} M_{i'j}^{n,k-1}\hat{\delta}S_{wm,(i',l),j'}^{n,k} + \partial_{\eta_{wm,i'j'}} M_{i'j}^{n,k-1}\hat{\delta}\eta_{wm,(i',l),j'}^{n,k}\right] = 0. \tag{24}$$

If we multiply Eq. 23 by $\delta\Phi_{wf,(i',l)}^{n,k}$ and Eq. 24 by $\delta S_{wf,(i',l)}^{n,k}$ and then add these equations to Eq. 22, the result would be identical to the matrix problem in Eq. 21. As a result, the matrix unknowns can be calculated by

$$\delta\Phi_{wm,i'j}^{n,k} = \bar{\delta}\Phi_{wm,i'j}^{n,k} + \sum_{l=1}^{N_{zf}}(\tilde{\delta}\Phi_{wm,(i',l),j}^{n,k}\delta\Phi_{wf,(i',l)}^{n,k} + \hat{\delta}\Phi_{wm,(i',l),j}^{n,k}\delta S_{wf,(i',l)}^{n,k}), \tag{25}$$

$$\delta S_{wm,i'j}^{n,k} = \bar{\delta}S_{wm,i'j}^{n,k} + \sum_{l=1}^{N_{zf}}(\tilde{\delta}S_{wm,(i',l),j}^{n,k}\delta\Phi_{wf,(i',l)}^{n,k} + \hat{\delta}S_{wm,(i',l),j}^{n,k}\delta S_{wf,(i',l)}^{n,k}), \tag{26}$$

$$\delta\eta_{wm,i'j}^{n,k} = \bar{\delta}\eta_{wm,i'j}^{n,k} + \sum_{l=1}^{N_{zf}}(\tilde{\delta}\eta_{wm,(i',l),j}^{n,k}\delta\Phi_{wf,(i',l)}^{n,k} + \hat{\delta}\eta_{wm,(i',l),j}^{n,k}\delta S_{wf,(i',l)}^{n,k}). \tag{27}$$

Eqs. 22 through 24 can be solved independently of the fracture system. Thus, we modify step 2a of the Newton Algorithm by first solving Eqs. 22 through 24. The changes in the fracture unknowns are then given by solving the fracture equations of Eq. 21, using implicitly definition of Eqs. 25 through 27. Subsequently, we explicitly use the changes in the fracture unknowns and Eqs. 25 through 27 to update the matrix δ-potential and matrix δ-saturation. Finally, the Newton iteration can be continued. This efficient numerical method is inexpensive as it only involves the solution of many

$(3\times N_m) \times (3\times N_m)$ matrices and the solution of a $(2\times N_f) \times (2\times N_f)$ matrix as opposed to a single big matrix. Therefore, not only the efficient numerical method reduces the computational time approximately by a factor of 14, but also it brings roughly a saving factor of 950 in computer memory.

A similar procedure can be given in order to develop an efficient numerical scheme for solving the upscaled equation including the non-equilibrium capillary potential by Hassanizadeh's approach. To do this, we replace the matrix effective water saturation η_{wm} everywhere it appears in Eqs. 20 through 27 by the dynamic capillary potential Φ_{wm}^{dyn}.

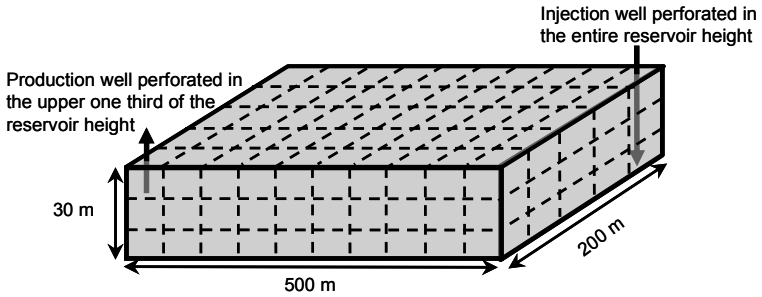

Fig. 3: Fractured reservoir waterflooding pattern.

Results and Discussion

In this Section, we present the results of the numerical simulation. It is important to note that all our results are only valid for truly fractured reservoirs, i.e., reservoirs for which the fracture permeability is one order of magnitude larger (with respect to the scaling ratio) than the matrix permeability. We consider a vertically fractured oil reservoir with a length of 500 m, width of 200 m, and height of 30 m. Initially, the reservoir is saturated with oil. The initial water saturation both in the fracture and in the matrix is equal to the irreducible water saturations ($S_{w,ir}$). As shown in Fig. 3, water is injected through the entire height of the reservoir from one corner and subsequently oil and water are produced through the upper third of the reservoir height at the diagonally opposite corner. Table 1 shows the basic input data for the numerical simulations. For each simulation case, the water injection rate is uniform. Table 2 shows the calculated global (effective) fracture permeabilities based on the different values of the lateral matrix-column size. Because fracture and matrix are considered as two different media, we use two different capillary-pressure and relative-permeability curves. Fig. 4 shows the capillary-pressure curves for the base case, i.e., contact angle of zero and completely water-wet. Fig. 5 shows the relative-permeability curves both for the fracture and for the matrix.

TABLE 1: Data Used in the Numerical Simulations.

Initial reservoir pressure (MPa)	27.5	Oil viscosity, μ_o (cp)	2
Bottomhole pressure in production wells (MPa)	26.9	Oil density, ρ_o (kg/m^3)	833
Well radius (m)	0.1524	Water viscosity, μ_w (cp)	0.5
Fracture aperture, δ (μm)	100	Water density, ρ_w (kg/m^3)	1025
Local fracture porosity, φ^*_f	1	Residual oil saturation in matrix, $S_{or,m}$	0.3
Intrinsic fracture permeability, k^*_f (D)	844	Residual oil saturation in fracture, $S_{or,f}$	0
Matrix porosity, φ_m	0.19	Irreducible water saturation in matrix, $S_{w,ir,m}$	0.25
Matrix permeability, k^*_m (mD)	1	Irreducible water saturation in fracture, $S_{w,ir,f}$	0

TABLE 2: Calculated Global Fracture Permeability and Porosity Based on Lateral Matrix-Column Sizes.

Lateral Matrix-Column Size, ℓ (m)	Global Fracture Permeability in the x- and y-direction, $k_{f,xy}$ (mD)	Global Fracture Permeability in the z-direction, $k_{f,z}$ (mD)	Global fracture porosity, φ_f
0.5	169	338	4×10^{-4}
2	42	84	1×10^{-4}
4	21	42	5×10^{-5}

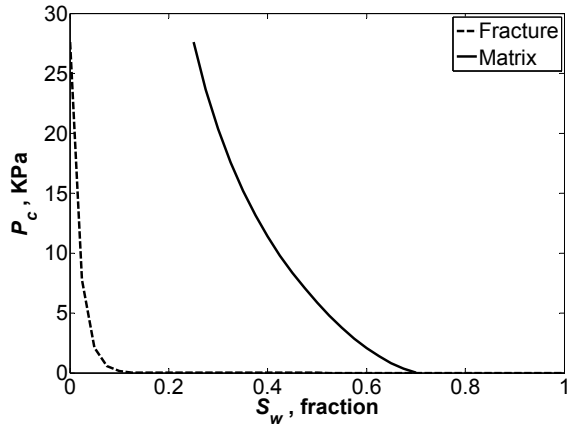

Fig. 4: Capillary-pressure curves versus water saturation.

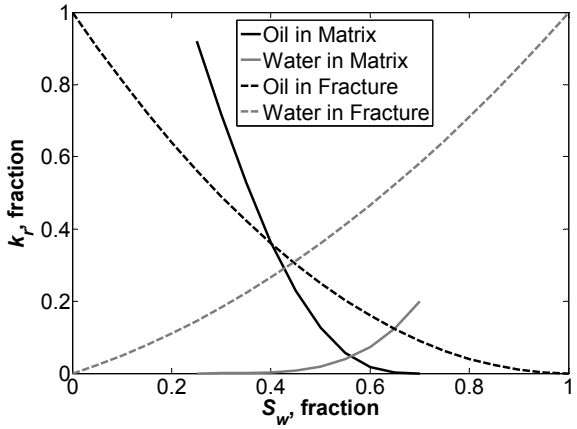

Fig. 5: Relative-permeability curves versus water saturation.

We discretize the fractured reservoir into 10×5×9 grid cells in the *x*-, *y*-, and *z*-direction. Hence, there are 450 grid cells for the fracture system, which contains 10×5 columns. Each column, which extends from the base rock to the cap rock, is subdivided in a stack of nine matrix blocks. In other words, corresponding to each fracture grid cell on the base plane, there is a single matrix column, consisting of a stack of nine matrix blocks. We use 9×9×9 grid cells in the *x*-, *y*-, and *z*-direction for each representative matrix column. Therefore, we have a total of 10×5×9 grid cells for the fracture part and (10×5×9)×9×9 grid cells to represent the matrix part leading to a total of 36900 grid blocks.

To demonstrate the capability of the upscaled-VFR model, we develop a fine-grid model, and compare the results of the fine-grid model with the results of the upscaled-VFR model. The fine-grid model (discrete fracture), which considers the fractures explicitly, includes 35,157,500 cells (703,150 cells for the fractures and 34,454,350 cells for the matrix system). The fine-grid model is a model that includes the fractures explicitly and hence is not an internal check of the validity of the numerical model.

We characterize the behavior of a VFR by considering the three most important dimensionless numbers. These dimensionless numbers are previously discussed in Salimi and Bruining (2009a, 2010a), but for reasons of easy reference, we briefly include the definition also in this paper. First, we define the Peclet number as the ratio of the capillary-diffusion time in the matrix columns and the residence time of the water in the fracture system. This Peclet number can be expressed as

$$Pe = \frac{\ell^2 u_{fw}}{D_{cap} L}, \quad \text{where} \quad D_{cap} = -\frac{\lambda_o \lambda_w}{\lambda_o + \lambda_w} \frac{\mathrm{d}P_c}{\mathrm{d}S_w}. \tag{28}$$

Here, ℓ is the lateral matrix-column size, u_{fw} is the water injection rate, λ_α is the mobility of phase α (oil, water), and L is the distance between wells. The capillary-diffusion coefficient D_{cap} is evaluated in the matrix domain. In Eq. 28, the capillary-diffusion coefficient is a strongly nonlinear function of the water saturation. Consequently, its values change with time and space. As mentioned above, the initial water saturation both in the fracture and in the matrix is equal to the irreducible water saturations ($S_{w,ir}$). Consequently, the capillary-diffusion coefficient (D_{cap} in Eq. 28) is initially zero for both the fracture and matrix, and remains zero at an early injection time for those regions that are far from the injection well. Therefore, if we use the geometric mean and/or harmonic mean, the average capillary-diffusion coefficient would become zero and/or infinity, respectively. However, for average over time, there is not such a problem. In addition, the geometric mean is a type of mean or average, which indicates the central tendency or typical value of a set of numbers, whereas the arithmetic mean is not a robust statistic, meaning that it is greatly influenced by outliers. This is the case for higher injection rates, because the injected water slightly penetrates to the matrix over long time of the simulation. Therefore, we use an arithmetic mean over the space and a geometric mean over time to obtain a single averaged value of the Peclet number for each case discussed below. The second dimensionless number is the gravity number that expresses gravity forces over viscous forces in the

fracture system. We use the following expression for this gravity number (Yortsos 1991; Shook et al. 1992)

$$N_{\mathrm{G}} = \frac{k_f \Delta\rho g H}{\mu_w u_{fw} L}, \tag{29}$$

where H is the height of the reservoir, k_f is the effective (global) fracture permeability, u_{fw} is the global water injection rate, and $\Delta\rho$ is the density difference between water and oil phase.

Comparison between the fine-grid model and the upscaled-VFR model

Here we give an example where we compared the results of the fine-grid model with the results of the upscaled-VFR model without including the non-equilibrium effects, i.e., $\tau_b = \tau_h = 0$. We assume the reservoir consists of identical matrix blocks of permeability $k_m = 1$ mD and size $\ell = 2$ m. Moreover, the fractures of the VFR configuration are assumed to have the same aperture. The input data for the fine-grid simulation are summarized in Table 1 (see also Figs. 4 and 5).

Figs. 6a and 6b show the cumulative oil production for a water injection rate of $q_w = 0.1$ PV/yr and $q_w = 1$ PV/yr, respectively. Using the matrix-block size of $\ell = 2$ m and the fracture aperture of 100 μm, the maximum error in oil recovery between the fine-grid model and the upscaled-VFR model is 2.66% for a water injection of $q_w = 0.1$ PV/yr at $t = 0.24$ PV. For a water injection rate of $q_w = 1$ PV/yr (Fig. 6b), the maximum relative error in oil recovery between the fine-grid simulation and the VFR model is 7.66% at $t = 0.31$ PV. We see from Fig. 6a that the cumulative oil production predicted by the upscaled-VFR model reaches almost the same value as the results of the fine-grid model. We also observe from Fig. 6b close agreement between the fine-grid and VFR model as the error in the cumulative oil production is 3.68% at the end of the simulation for $q_w = 1$ PV/yr. Moreover, for higher injection rates and consequently larger Peclet numbers, the discrepancy between the fine-grid results and the upscaled-VFR results is also larger. The reason for this observation is that the numerical dispersion of the upscaled-VFR model for the same time and space discretization is larger for a higher injection rate than for a lower injection rate, because the numerical dispersion is approximately proportional to the velocity. Therefore, whenever the fluid velocity in the fractures increases, the numerical dispersion induced by the upscaled model increases as well. Moreover, the rate of transport by convection in the fracture is also higher, meaning that the residence time for water in the fracture is short. Therefore, the capillary-diffusion process in the fracture becomes slower than the convection transport in the fracture. The comparison between the fine-grid results and upscaled-VFR results shows that the upscaled-VFR model can give physically reasonable results, though some differences between the upscaled-VFR model and the fine-grid simulation can be seen. The upscaled-VFR model contains 76,050 cells, which represents approximately a reduction factor of 460 relative to the fine-grid (discrete fracture) model with 35,157,500. For the above-mentioned cases, the fine-grid model requires about 40 days, while the upscaled-VFR model needs approximately 10 hours. Therefore, the speed up in this case is roughly 100.

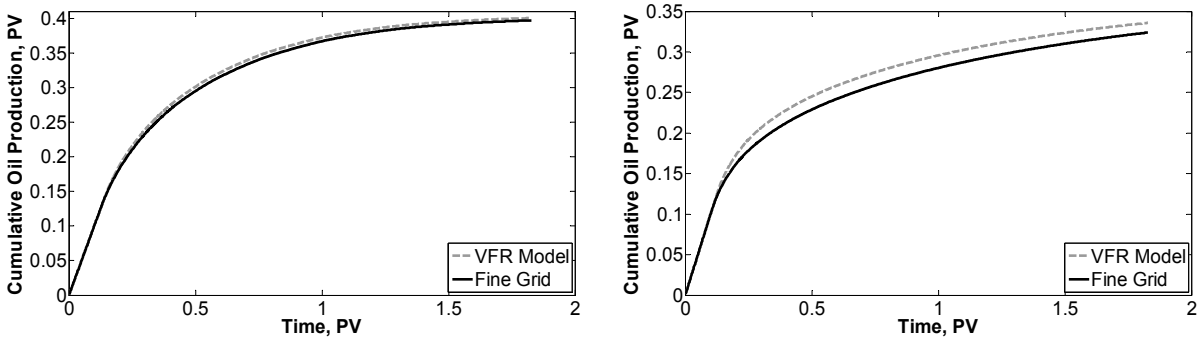

Fig. 6: Cumulative oil production as a function of PV water injected for (a) water injection rate of $q_w = 0.1$ PV/yr and $\ell = 2$ m, and (b) water injection rate of $q_w = 1$ PV/yr and $\ell = 2$ m.

Fig. 7 shows the oil saturation history after water injection in the two NE corner columns, with production in the top 1/3 of the two SW corner columns. The water saturation first expands via the bottom of the reservoir. We observe in Fig. 7 that co-current (gravity) and counter-current imbibition occur at the same time.

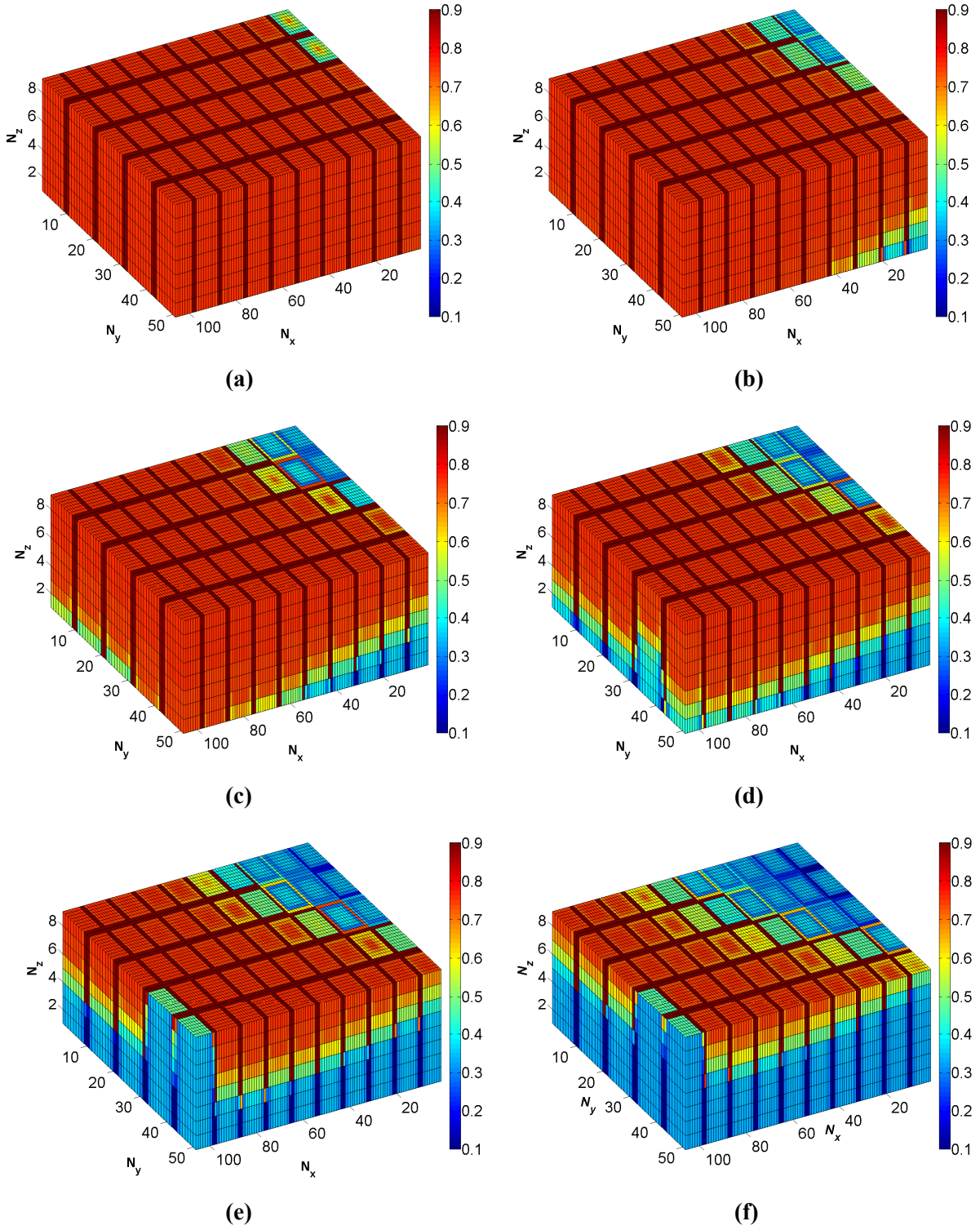

Fig. 7: Oil Saturation history at (**a**) t = 50 days, (**b**) t = 375 days, (**c**) t = 675 days, (**d**) t = 750 days, (**e**) t = 1250 days, and (**f**) t = 2000 days. The reservoir has a length of 500 m in the x-direction, 200 m in the y-direction and 30 m in the z-direction. The water injection rate is 0.1 PV/yr and the lateral matrix column size is 0.5 m. First, the water occupies the bottom of the reservoir. Then, the water rises in the fractures and finally the water rises in the columns. Due to gravity, the oil at the top of the reservoir is not fully depleted

Effect of the Non-Equilibrium

The non-equilibrium behavior changes the capillary-pressure and relative permeability behavior as explained above. In Barenblatt's theory, the time to reach equilibrium (delay time) is denoted by τ_b, and in Hassanizadeh's theory, the characteristic parameter that indicates the importance of the non-equilibrium effect is the capillary-damping coefficient τ_h. Fig. 8a shows the effect of the delay time on the cumulative oil production for a water injection rate of $q_w = 0.1$ PV/yr and a lateral matrix-column size of $\ell = 0.5$ m. Here, we describe the oil recovery ratio between non-zero delay-time cases and the zero delay-time case. We observe in Fig. 8a that the delay time does not influence oil recovery substantially. The reason is that for low injection rates and thus low Peclet numbers (Fig. 8a, $Pe \approx 0.06$), the residence time of water in the fracture (i.e., 0.25 PV or 913 days) is much longer than any reasonable delay time τ_b. The residence time is the time at which the cumulative oil production curve starts to deviate considerably from the initial straight line. In this case, the effect of the delay time is almost zero. On the other hand, we observe from Fig. 8b that at high Peclet numbers, the delay time affects oil production significantly. Moreover, Fig. 8b reveals that significant water breakthrough immediately occurs for non-zero delay-time cases. As a result, the recovery ratio starts decreasing from the beginning until it reaches its minimum value of 0.37, 0.16, and 0.06 respectively for $\tau_b = 10^6$ sec, 3×10^6 sec, and 10^7 sec at $t = 0.1$ PV, the time at which water breakthrough occurs for $\tau_b = 0$. Subsequently, the recovery ratio increases and reaches a value of 0.95, 0.80, and 0.45 respectively for $\tau_b = 10^6$ sec, 3×10^6 sec, and 10^7 sec at $t = 1.83$ PV. For high Peclet numbers ($Pe \approx 300$), the residence time of water in the fractures is short, i.e., of the order of 0.1 PV or 3.65 days. In each of the non-zero delay-time cases shown in Fig. 8b, the delay time is much larger than the residence time and thus it influences the cumulative oil production considerably, as expected.

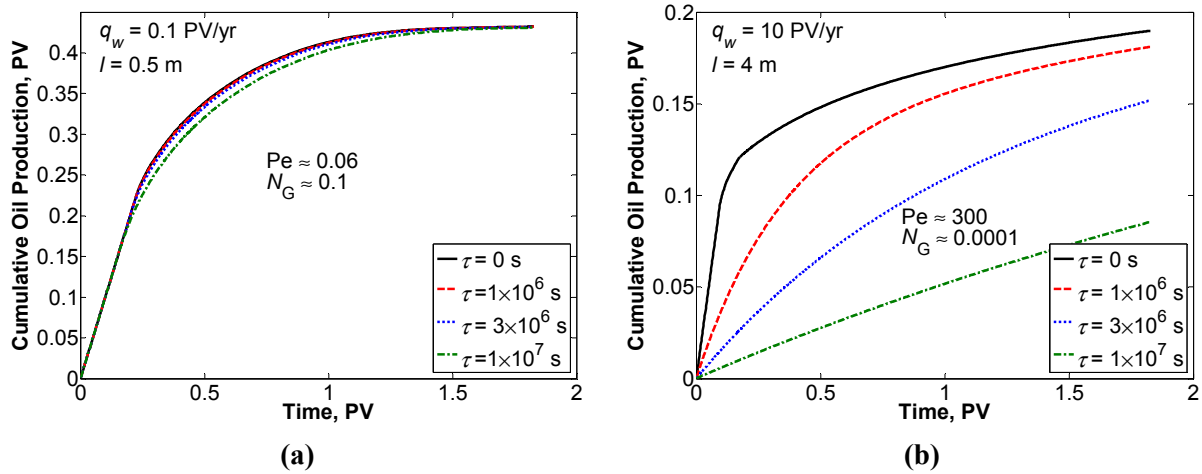

Fig. 8: Effect of the delay time on the cumulative oil production for (a) water injection rate $q_w = 0.1$ PV/yr and lateral matrix-column size of $\ell = 0.5$ m, and (b) water injection rate of $q_w = 10$ PV/yr and lateral matrix-column size of $\ell = 4$ m.

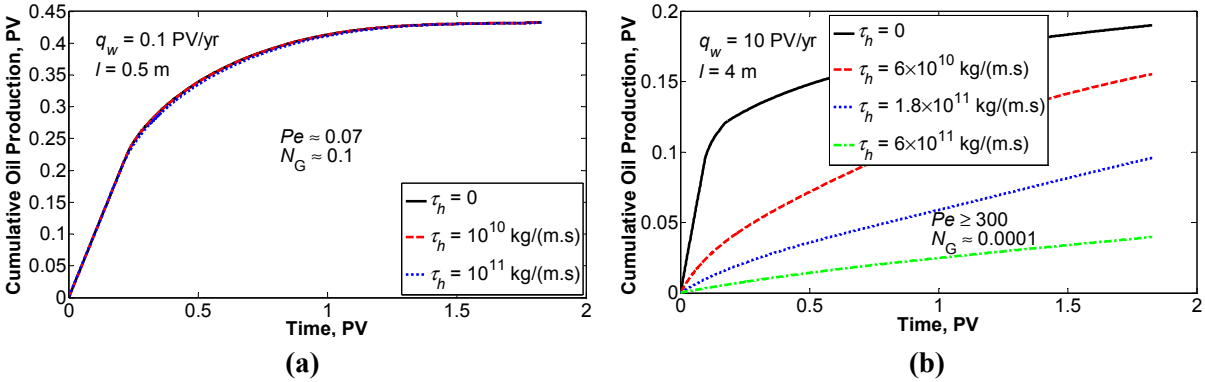

Fig. 9: Effect of the capillary-damping coefficient on the cumulative oil production for (a) water injection rate $q_w = 0.1$ PV/yr and lateral matrix-column size of $\ell = 0.5$ m, and (b) water injection rate of $q_w = 10$ PV/yr and lateral matrix-column size of $\ell = 4$ m.

Figs. 9a and 9b describe the non-equilibrium effects of Hassanizadeh's theory (capillary-damping coefficient) on the cumulative oil production for a water injection rate of q_w = 0.1 PV/yr and a lateral matrix-column size of ℓ = 0.5 m, and for q_w = 10 PV/yr and ℓ = 4 m, respectively. In the same way as for the delay-time effects (Fig. 8a), we observe in Fig. 9a that at low Peclet numbers (Pe < 0.07), the dynamic capillary pressure for the range of the capillary-damping coefficient (τ_h) between 0 and 10^{11} kg/(m.s) does not considerably influence oil recovery. However, Fig. 9b shows that the dynamic capillary pressure does have noticeable effects on oil recovery and illustrates approximately the same behavior of the non-equilibrium effects for Hassanizadeh's theory as for Barenblatt's theory (Fig. 8b). As revealed in Fig. 9b, the recovery ratio reaches a value of 0.82, 0.50, and 0.21 respectively for $\tau_h = 6\times10^{10}$ kg/(m.s), 1.8×10^{11} kg/(m.s), and 6×10^{11} kg/(m.s) at t = 1.83 PV. Again, the reason for having significant effects of the dynamic capillary pressure at high Peclet numbers is that the oil recovery mechanism in this regime is limited by the rate of imbibition from the matrix system.

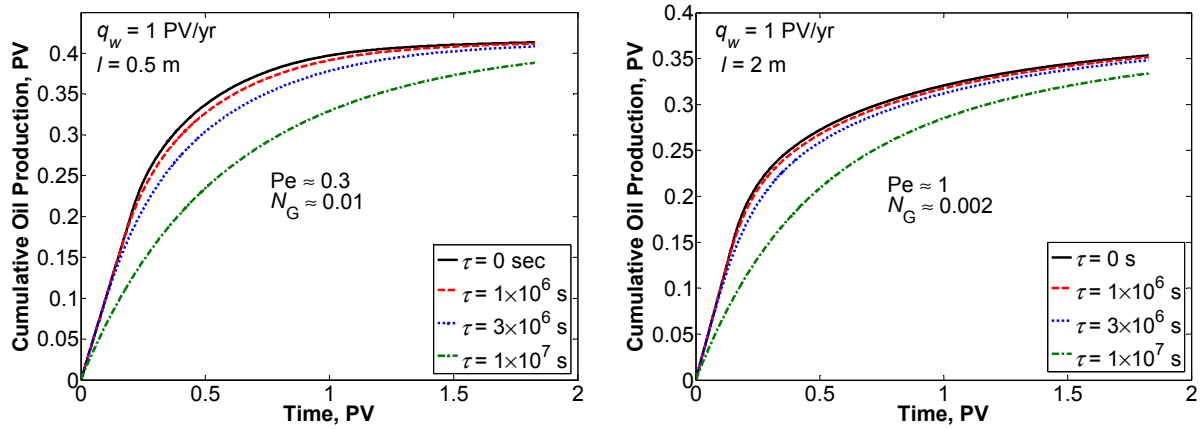

Fig. 10: Effect of the delay time on the cumulative oil production at a water injection rate q_w = 1 PV/yr for (a) lateral matrix-column size of ℓ = 0.5 m and (b) lateral matrix-column size of ℓ = 2 m.

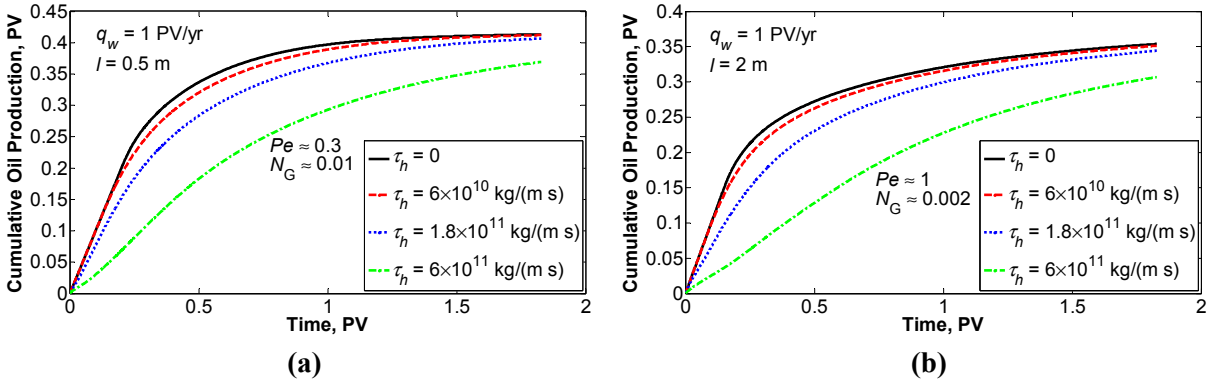

Fig. 11: Effect of the capillary-damping coefficient on the cumulative oil production at a water injection rate q_w = 1 PV/yr for (a) lateral matrix-column size of ℓ = 0.5 m and (b) lateral matrix-column size of ℓ = 2 m.

For intermediate Peclet numbers we distinguish two cases; one with small (ℓ = 0.5 m) and one with large (ℓ = 2 m) lateral matrix columns. Figs. 10a and 10b show the effect of the delay time on the cumulative oil production for a water injection rate of q_w = 1 PV/yr and a lateral matrix-column size of ℓ = 0.5 m and ℓ = 2 m, respectively. The size of the matrix columns has an influence on the fracture spacing and hence the global fracture permeability (see Eq. 15). Therefore, this has also an effect on the gravity number (0.01 vs. 0.002). Moreover, the size of matrix-column size influences the Peclet number as well (0.3 vs. 1, see Eq. 28). We observe from Figs. 10a and 10b that the residence time of water is about 0.25 PV (90 days) and 0.18 PV (66 days), respectively. This is also reflected by the fact that the Peclet number for the ℓ = 0.5 m case ($Pe \approx 0.3$) is smaller than for the ℓ = 2 m case ($Pe \approx 1$). Figs. 10a and 10b reveal that the difference between the results for $\tau_b = 10^6$ sec and 3×10^6 sec is almost negligible, whereas for the longest delay time (10^7 sec), there is an appreciable effect of the

delay time. For intermediate Peclet numbers, the residence time of the fluids and the delay time are of the same order of magnitude, meaning that for sufficiently long delay times ($\tau_b = 10^7$ sec or 116 days), the behavior is completely different from the behavior of short delay times. As shown in Fig. 10a, the results for high gravity numbers show a somewhat larger dependence on the delay time than for small gravity numbers (Fig. 10b).

The general pattern observed in Figs. 10a and 10b reoccurs in Figs. 11a and 11b for the non-equilibrium effects of Hassanizadeh's theory.

To emphasize the effect of the delay time on the displacement mechanism, we show the oil saturation profiles in Figs. 12a and 12b for a water injection rate of $q_w = 1$ PV/yr without delay time and with a delay time of $\tau_b = 10^7$ sec at $t = 50$ days, respectively. Fig 11a, for zero delay times, clearly illustrates that the waterfront is still far from the production well and water penetrates more into the matrix columns nearby the injection well, while Fig 11b with $\tau_b = 10^7$ sec describes that water breakthrough has already occurred.

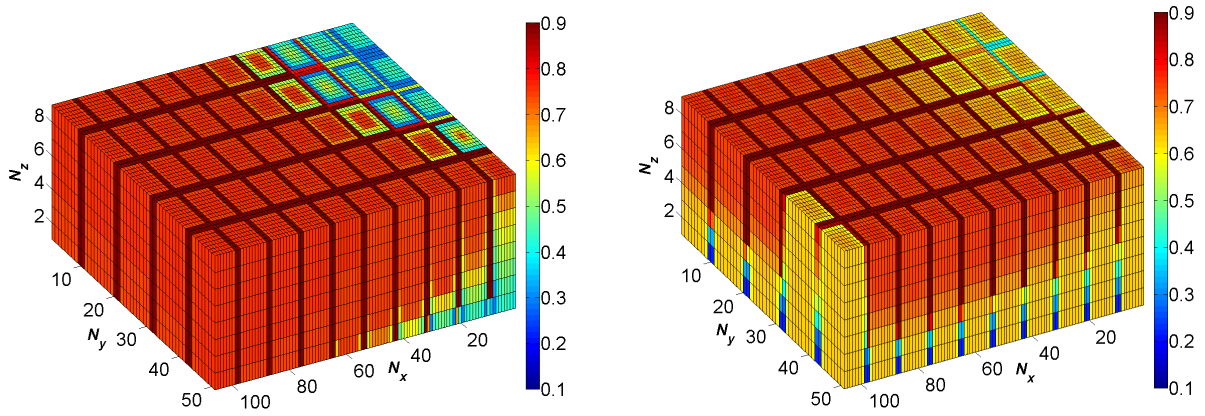

(a) **(b)**

Fig. 12: Oil saturation profiles for a water injection rate of $q_w = 1$ PV/yr and a lateral matrix-column size of $\ell = 0.5$ m at $t = 50$ days for (a) $\tau_b = 0$ sec and (b) $\tau_b = 10^7$ sec.

The non-equilibrium effects have consequences for laboratory experiments. In the laboratory, a typical cylindrical core has a length of 20 cm and a diameter of 10 cm. Also, a usual injection rate is 5 ml/min. To be able to calculate the Peclet number; we need to estimate the capillary-diffusion coefficient. We assume that the absolute permeability of the core is 1 mD. Moreover, we use the matrix relative permeability functions that are plotted in Fig. 5, and the average capillary derivative and the average mobility factor $[\lambda_o\lambda_w/(\lambda_o+\lambda_w)]$ for calculating D_{cap}. Note that the characteristic length for the capillary diffusion and convection transport in a laboratory core is the same. Therefore, the definition for the Peclet number in Eq. 28 reduces to $Pe_{lab} = U_{inj}\, L/D_{cap}$. For the laboratory specifications mentioned above, the calculated Peclet number would be $Pe_{lab} = 1768$. Therefore, most of the laboratory experiments are in the high-Peclet-number regime. As a result, the non-equilibrium effects have considerable effects on the rate of oil production. Consequently, in the laboratory, samples with long delay times and/or large capillary-damping coefficients are often erroneously considered oil-wet. This has consequences for any remediative action (Puntervold and Austad 2008; Puntervold et al. 2009) to enhance the imbibition rates.

Comparison between Barenblatt's and Hassanizadeh's Approach

Figs. 13a and 13b show a comparison of the cumulative oil production between the non-equilibrium model by Barenblatt and the non-equilibrium model by Hassanizadeh for a water injection rate of $q_w = 1$ PV/yr and a lateral-matrix-column size of $\ell = 0.5$ m and for a water injection rate of $q_w = 10$ PV/yr and a lateral-matrix-column of $\ell = 4$ m, respectively. Figs. 13a and 13b present three pairs of cases. Note that for each pair of this comparison, we use Eq. 11 to relate the delay time (τ_b) of Barenblatt's approach to the capillary-damping coefficient (τ_h) of Hassanizadeh's approach. Using the

matrix capillary pressure function shown in Fig. 5, the average capillary derivative (Λ) is 60 kPa. Figs. 13a and 13b clearly reveal that for each pair of the comparison, the cumulative oil production for the non-equilibrium effects of Hassanizadeh is larger than that for the non-equilibrium effects of Barenblatt. Moreover, the discrepancy between Barenblatt's and Hassanizadeh's approach for each pair shown in Fig.12a is smaller than that shown in Fig.12b. The main reason is that at a smaller lateral matrix-column size of ℓ = 0.5 m and a lower water injection rate q_w = 1 PV/yr (i.e., Fig. 13a), the corresponding Peclet number is smaller than that for ℓ = 4 m and q_w = 10 PV/yr (Fig. 13b). As a result, for ℓ = 0.5 m and q_w = 1 PV/yr, the rate of imbibition is faster and the residence time of fluids in the fracture system is longer. Therefore, the non-equilibrium effects is less pronounced for ℓ = 0.5 m and q_w = 1 PV/yr illustrated in Fig. 13a. As the Peclet number increases, the difference between Barenblatt's and Hassanizadeh's approach would also become larger.

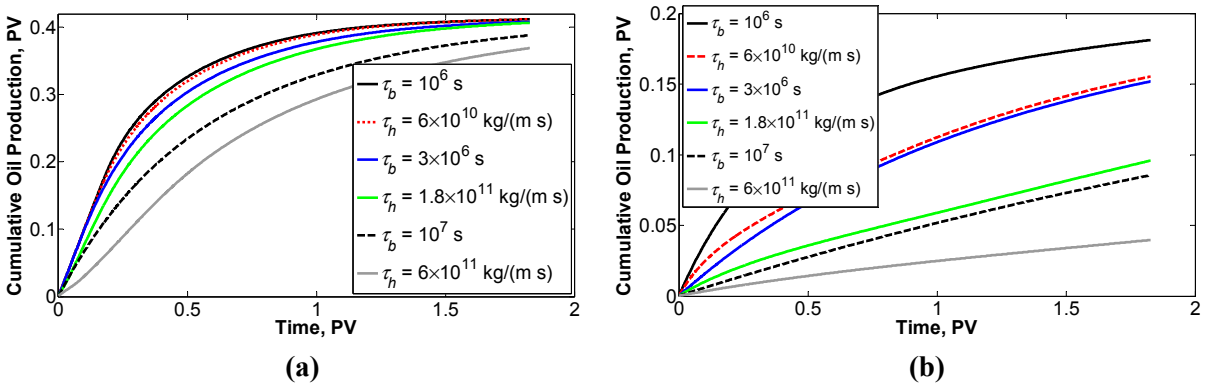

Fig. 13: Comparison of the cumulative oil production between Barenblatt's and Hassanizadeh's theory. (a) For a water injection rate of q_w = 1 PV/yr and a lateral matrix-column size of ℓ = 0.5 m. (b) For a water injection rate of q_w = 10 PV/yr and a lateral matrix-column size of ℓ = 4 m.

Another reason for having discrepancies between Barenblatt's and Hassanizadeh's approach is that the non-equilibrium model of Hassanizadeh does not deal with relative permeabilities, whereas the non-equilibrium theory of Barenblatt modifies relative permeabilities.

In general, the results shown in Figs. 13a and 13b indicate the fact that the non-equilibrium theory of Hassanizadeh cannot be related to Barenblatt's approach if constant values of τ_b and τ_h are used. Even if varying values of τ_b and τ_h were used, it is almost impossible to obtain a relation between the delay time (τ_b) and the capillary-damping coefficient (τ_b) to be able to get quantitatively the same results; because (1) capillary pressures are always non-linear functions and (2) the non-equilibrium effects of relative permeabilities of Barenblatt's approach does not exist in Hassanizadeh's theory. However, both approaches illustrate qualitatively the importance of the non-equilibrium effects in terms of oil recovery from fractured reservoirs.

The salient features of the upscaled-VFR model including the non-equilibrium effects are summarized in Fig. 14, where the cumulative oil production at 1 PV is plotted versus the Peclet number (*Pe*) and the gravity number (N_G) for various delay times. At small gravity numbers and large Peclet numbers, the recovery is low. The recovery at small gravity numbers is rather insensitive to the Peclet number. As the gravity number increases and the Peclet number decreases, the recovery becomes much higher. It can be expected that here counter-current imbibition is replaced by the much more effective co-current gravity imbibition. Also, the rate of imbibition from the matrix column becomes larger compared to the rate of fluid transport in the fracture system. In the absence of delay times, the maximum recovery becomes higher than when delay times are relevant. At a critical value of the gravity number-Peclet number, there is a sudden decrease in oil recovery when delay times are ignored. Therefore, there is a smooth transition between the two regimes, from small to large Peclet numbers. At high Peclet numbers, the rate of oil production becomes limited by imbibition from the matrix column and hence by the delay time. One may speculate that the transition where the result is independent of the imbibition rate, due to long residence times of fluids in the fracture, to the situation at large Peclet numbers where it does become sensitive to the imbibition rate is unstable. For this reason, in the absence of delay times, a peak of relative high oil recovery occurs.

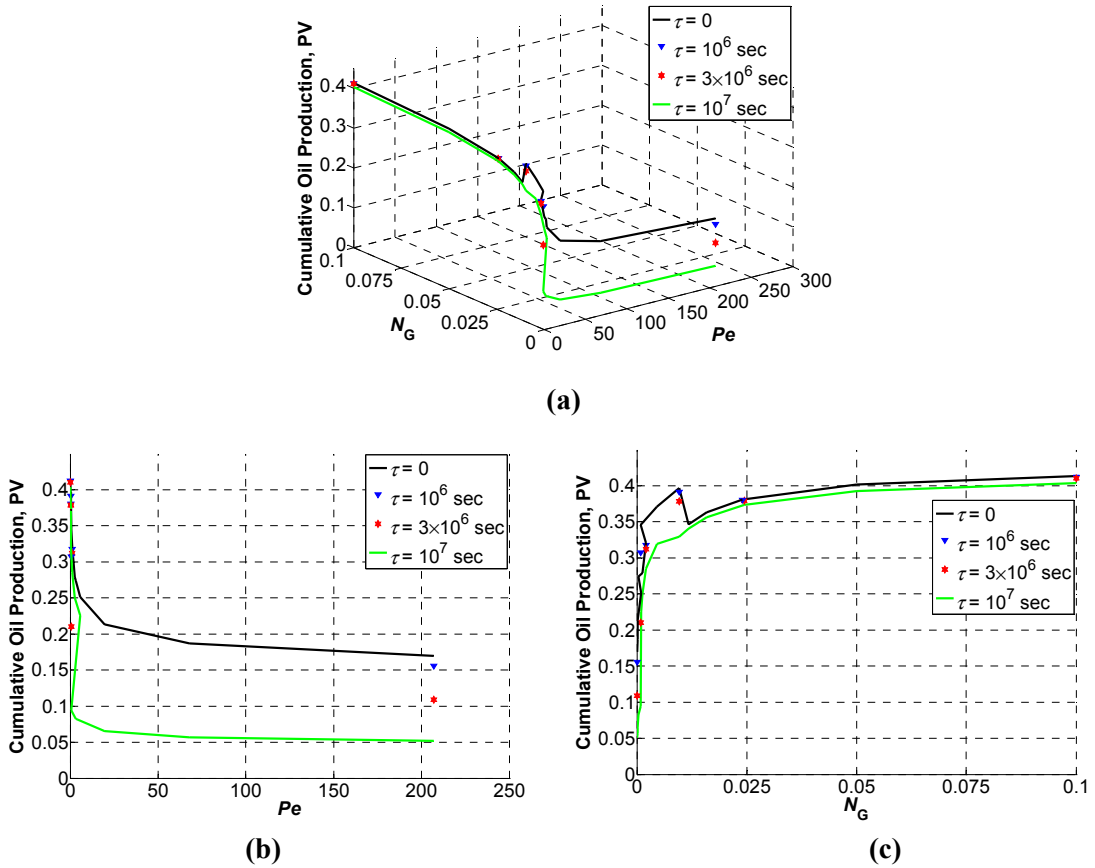

Fig. 14: Cumulative oil production at one PV injected water (a) versus the gravity number (N_G) and the Peclet number (Pe), (b) projected on the cumulative oil production-Peclet plane, (c) projected on the cumulative oil production-gravity number plane.

Conclusions

- We derive a physically based upscaled model in which the non-equilibrium effect is included for the vertically fractured reservoir (VFR) using homogenization.
- We develop a computationally efficient numerical scheme to solve the upscaled-VFR model.
- At low Peclet numbers, the rate of imbibition dominates over the convective transport in the fracture. Therefore, the characteristic time of fluid-flow exchange at the boundary between fracture and matrix is short with respect to the residence time of water in the fracture. Hence, the water cut is small.
- At high Peclet numbers, the convective transport is dominant over imbibition and hence the oil recovery mechanism is controlled by the rate of imbibition. Furthermore, the residence time of water is much shorter than the characteristic time of imbibition. As a result, less fluid-flow exchange occurs for the same amount of injected water. Thus, if we were in the high Peclet number regime, the recovery would be low accordingly. Hence, the water cut is large.
- If the residence time of water in the fractured reservoir is much longer than the delay time τ_b, the delay time (non-equilibrium effects) does not influence oil recovery qualitatively. Conversely, for large Peclet numbers, the residence time of water in the fractures is short and hence high values of τ_b and τ_h significantly slow down the oil recovery due to the non-equilibrium effects.
- In general, due to the non-linear nature of the capillary pressure function, it is not possible to find a relation between the delay time (Barenblatt) and the capillary-damping coefficient (Hassanizadeh) and consequently to make a direct comparison between the two descriptions. Even if the results between the description of Barenblatt and Hassanizadeh cannot be directly compared, the

qualitative behavior is the same and both approaches show the importance of taking into account the non-equilibrium effects in the capillary-pressure and relative permeability behavior.

- It is asserted that in partially water-wet systems, the values of the delay time τ_b can be long (of the order of 100 days) due to the fact that first an oil film must be removed from the corrugated surface of the grains by a combined dissolution diffusion process. Correspondingly, also the capillary-damping coefficient τ_h can be high.
- Experiments in the laboratory are expected to be more sensitive to non-equilibrium capillary-pressure effects as Peclet numbers are usually high. The delay time τ_b can easily exceed the experimentation time. It is important to distinguish between truly oil-wet systems and systems that are water-wet with long delay times.

In view of the transparent physical basis of homogenization, we assert that improved fracture modeling can be achieved using the upscaled-VFR model. Based on the comparison between the fine-grid model and the upscaled-VFR model, the upscaled-VFR model is capable to predict oil recovery accurately.

Acknowledgment

We thank Statoil-Hydro for supporting our research on oil recovery from fractured reservoirs. We also thank Sharif University of Technology for their steady collaboration and the National Iranian Oil Company (NIOC) for continuous support of this work. We acknowledge Maryam Namdar Zanganeh, William R. Rossen, Stefan M. Luthi, and Giovanni Bertotti for many useful discussions and comments. We also acknowledge SPE for granting the Nico van Wingen Memorial Graduate Fellowship in Petroleum Engineering to the first author.

References

Aguilera, R. 1998. Geological Aspects of Naturally Fractured Reservoirs. *The Leading Age* **17** (12): 1667-1670.

Al-Harbi, M., Cheng, H., He, Z., and Datta-Gupta, A. 2005. Streamline-Based Production Data Integration in Naturally Fractured Reservoirs. *SPE J.* **10** (4): 426-439.

Al-Huthali, A. and Datta-Gupta, A. 2004. Streamline Simulation of Counter-Current Imbibition in Naturally Fractured Reservoirs. *J. Pet. Sci. Eng.* **43** (3-4): 271-300.

Anderson, W.G. 1987. Wettability Literature Survey-Part 6: The Effects of Wettability on Waterflooding. *J. Pet Tech* **39** (12): 1605-1622.

Arbogast, T. 1993. Gravitational Forces in Dual-Porosity Systems: I. Model Derivation by Homogenization. *Transp. Porous Media* **13** (2): 179-203.

Balogun, A., Kazemi, H., Ozkan, E., Al-Kobaisi, M., and Ramirez, B. 2009. Verification and proper Use of Water-Oil Transfer Function for Dual-Porosity and Dual-Permeability Reservoirs. *SPE Res Eval & Eng* **12** (2): 189-199. SPE-104580-PA.

Barenblatt, G.I., Zheltov, Iu.P., and Kochina, I.N. 1960. Basic Concept in the Theory of Seepage of Homogeneous Liquids in Fissured Rocks. *J. of Applied Mathematics and Mechanics* **24** (5): 1286-1303.

Barenblatt, G.I. 1971. Filtration of Two Nonmixing Fluids in a Homogeneous Porous Medium. *Soviet Academy Izvestia. Mechanics of Gas and Fluids* **5**: 857–864.

Barenblatt, G.I. and Gilman, A.A. 1987. Nonequilibrium Counterflow Capillary Impregnation. *J. Eng. Phys.* **52** (3): 335-339.

Barenblatt, G.I., Garcia-Azorero, J., De Pablo, A., and Vazquez, J.L. 1997. Mathematical Model of the Non-Equilibrium Water-Oil Displacement in Porous Strata. *Applicable Analysis* **65**: 19–45.

Barenblatt, G.I., Patzek, T.W., and Silin, D.B. 2003. The mathematical Model of Nonequilibrium Effects in Water-Oil Displacement. *SPE J.* **8** (4): 409-416. SPE-87329-PA.

Behbahani, H. and Blunt, M.J. 2005. Analysis of Imbibition in Mixed-Wet Rocks Using Pore-Scale Modeling. *SPE J.* **10** (4): 466-473. SPE-90132-PA.

Dahan, O., Nativ, R., Adar, E., and Berkowitz, B. 1998. A Measurement System to Determine Water Flux and Solute Transport through Fractures in the Unsaturated Zone. *Ground Water* **36** (3): 444-449.

Douglas, J. Jr., Hensley, J.L., and Arbogast, T. 1991. A Dual-Porosity Model for Waterflooding in Naturally Fractured Reservoirs. *Comput. Meth. Appl. Mech. Eng.* **87** (2-3): 157-174.

Elzeftawy, A. and Mansell, R.S. 1975. Hydraulic Conductivity Calculations for Unsaturated Steady-State and Transient-State Flow in Sands. *Soil Sci. Soc. Am. Proc.* **39**: 599-603.

Finkbeiner, T., Barton, C.A., and Zoback, M.D. 1997. Relationships among In-Situ Stress, Fractures and Faults, and Fluid Flow: Monterey Formation, Santa Maria Basin, California. *American Association of Petroleum Geologists Bulletin* **81** (12): 1975-1999.

Firoozabadi, A. 2000. Recovery Mechanisms in Fractured Reservoirs and Field Performance. *J. Cdn. Pet. Tech.* **39** (11): 13-17.

Graue, A., Bognø, T., Baldwin, B.A., and Spinler, E.A. 2001. Wettability Effects on Oil-Recovery Mechanisms in Fractured Reservoirs. *SPE Res Eval & Eng* **4** (6): 455-465. SPE-74335-PA.

Hassanizadeh, S.M. and Gray, W.G. 1990. Mechanics and Thermodynamics of Multiphase Flow in Porous Media Including Interphase Boundaries. *Adv. Water Resour.* **13** (4): 169-186.

Hassanizadeh, S.M. and Gray, W.G. 1993. Thermodynamic Basis of Capillary Pressure in Porous Media. *Water Resour. Res.* **29** (10): 3389-3405.

Hassanizadeh, S.M., Celia, M.A., and Dahle, H.K. 2002. Dynamic Effect in the Capillary Pressure-Saturation Relationship and Its Impact on Unsaturated Flow. *Vadose Zone J.* **1**: 38-57.

Hatiboglu, C.U. and Babadagli, T. 2007. Oil Recovery by Counter-Current Spontaneous Imbibition: Effects of Matrix Shape Factor, Gravity, IFT, Oil Viscosity, Wettability, and Rock Type. *J. Pet. Sci. Eng.* **59** (1-2): 106-122.

Karimaie, H. and Torsæter, O. 2007. Effect of Injection Rate, Initial Water Saturation and Gravity on Water Injection in Slightly Water-Wet Fractured Porous Media. *J. Pet. Sci. Eng.* **58** (1-2): 293-308.

Kazemi, H. 1969. The Interpretation of Interference Tests in Naturally Fractured Reservoirs with Uniform Fracture Distribution. *SPE J.* **9** (4): 451-462. SPE-2156-A.

Kazemi, H., Gilman, J.R., and Elasharkawy, A.M. 1992. Analytical and Numerical Solution of Oil Recovery from Fractured Reservoirs with Empirical Transfer Functions. *SPE Res Eng* **7** (2): 219-227.

Leverett, M.C. Flow of Oil-Water Mixtures through Unconsolidated Sands. 1939. *Trans.*, AIME **132**: 149-171.

Morrow, N.R. and Mason, G. 2001. Recovery of Oil by Spontaneous Imbibition. *Curr. Opin. Colloid Interface Sci.* **6** (4): 321-337.

Muskat, M. and Meres, M.W. 1936. The Flow of Heterogeneous Fluids through Porous Media. *J. Appl. Phys.* **7** (921): 346-363.

Nelson, R.A. 2001. *Geologic Analysis of Naturally Fractured Reservoirs*, second edition. Woburn, USA: Gulf Professional Publishing.

Pavone, D.R. 1990. A Darcy's Law Extension and a New Capillary Pressure Equation for Two-Phase Flow in Porous Media. Paper SPE 20474 presented at the SPE Annual Technical Conference and Exhibition, New Orleans, Louisiana, 23-26 September. SPE-20474-MS.

Plug, W.J. and Bruining. J. 2007. Capillary Pressure for the Sand-CO_2-Water System under Various Pressure Conditions. Application to CO_2 Sequestration. *Adv. Water Resour.* **30** (11): 2339-2353.

Plug, W.J., Mazumder, S., and Bruining, J. 2008. Capillary Pressure and Wettability Behavior of CO_2 Sequestration in Coal at Elevated Pressures. *SPE J.* **13** (4): 455-464. SPE-108161-PA.

Pooladi-Darvish, M. and Firoozabadi, A. 2000. Cocurrent and Countercurrent Imbibition in a Water-Wet Matrix Block. *SPE J.* **5** (1): 3-11. SPE-38443-PA.

Puntervold, T. and Austad, T. 2008. Injection of Seawater and Mixtures with Produced Water into North Sea Chalk Formation: Impact of Fluid-Rock Interactions on Wettability and Scale Formation. *J. Pet. Sci. Eng.* **63** (1-4): 23-33.

Puntervold, T., Strand, S., and Austad, T. 2009. Coinjection of Seawater and Produced Water to Improve Oil Recovery from Fractured North Sea Chalk Oil Reservoirs. *Energy and Fuels* **23** (5): 2527-2536.

Rangel-German, E.R. and Kovscek, A.R. 2002. Experimental and Analytical Study of Multidimensional Imbibition in Fractured Porous Media. *J. Pet. Sci. Eng.* **36** (1-2): 45-60.

Saidi, A.M. 1983. Simulation of Naturally Fractured Reservoirs. Paper SPE 12270 presented at the SPE Reservoir Simulation Symposium, San Francisco, California, 15-18 November.

Salimi, H. and Bruining, J. 2008. Improved Prediction of Oil Recovery from Waterflooded Fractured Reservoirs. Paper SPE 115361 presented at the SPE Annual Technical Conference and Exhibition, Denver, Colorado, 21-24 September. doi: 10.2118/115361-MS.

Salimi, H. and Bruining, H. 2009a. Upscaling in Vertically Fractured Oil Reservoirs Using Homogenization. *Transp. Porous Media*. doi: 10.1007/s11242-009-9483-1.

Salimi, H. and Bruining, J. 2009b. Upscaling in Partially Fractured Oil Reservoirs Using Homogenization. Paper SPE 125559 presented at the SPE/EAGE Reservoir Characterization and Simulation Conference, Abu Dhabi, UAE, 19-21 October. doi: 10.2118/125559-MS.

Salimi, H. and Bruining, J. 2010a. Improved Prediction of Oil Recovery from Waterflooded Fractured Reservoirs Using Homogenization. *SPE Res Eval & Eng* **13** (1): 44-55. SPE-115361-PA.

Salimi, H. and Bruining, J. 2010b. The Influence of Heterogeneity, Wettability, and Viscosity Ratio on Oil Recovery from Vertically Fractured Oil Reservoirs. Accepted for publication in *SPE Journal*. SPE-140152-PA. doi: 10.2118/140152-PA.

Sarma, P. and Aziz, K. 2006. New Transfer Function for Simulation of Naturally Fractured Reservoirs with Dual-Porosity Models. *SPE J.* **11** (3): 328-340.

Seethepalli, A., Adibhatla, B., and Mohanty, K.K. 2004. Physicochemical Interactions During Surfactants Flooding of Fractured Carbonate Reservoirs. *SPE J.* **9** (4): 411-418. SPE-89423-PA.

Shook, M., Li, D., and Lake, L.W. 1992. Scaling Immiscible Flow through Permeable Media by Inspectional Analysis. *In SITU* **16** (4): 311-349.

Siemons, N., Bruining, J., Castelijns, H., and Wolf, K.H. 2006. Pressure Dependence of the Contact Angle in a CO_2-H_2O-Coal System. *J. Colloid Interface Sci.* **297** (2): 755-761.

Smiles, D.E., Vachaud, G., and Vauclin, M. 1971. A Test of the Uniqueness of the Soil Moisture Characteristic During Trabsient, Non-Hysteretic Flow of Water in a Rigid Soil. *Soil Sci. Soc. Am. Proc.* **35**: 535-539.

Sonier, F., Souillard, P., and Blaskovich, F.T. 1988. Numerical Simulation of Naturally Fractured Reservoirs. *SPE Res Eng* **3** (4): 1114-1122.

Stauffer, F. 1978. Time Dependence of the Relations Between Capillary Pressure, Water Content and Conductivity During Drainage of Porous Media. IAHR Symposium on Scale Effects in Porous Media, Thessaloniki, Greece, 29 August-l September.

Tang, G-Q. and Firoozabadi, A. 2001. Effect of Pressure Gradient and Initial Water Saturation on Water Injection in Water-Wet and Mixed-Wet Fractured Porous Media. *SPE Res Eval & Eng* **4** (6): 516-524. SPE-74711-PA.

Teixell, A., Durney, D.W., and Arboleya, M.L. 2000. Stress and Fluid Control on Decollement within Competent Limestone. *Journal of Structural Geology* **22** (3): 349-371.

Topp, G.C., Klute, A., and Peters, D.B. 1967. Comparison of Water Content-Pressure Head Data Obtained by Equilibrium, Steady-State and Unsteady-State Methods. *Soil Sci. Soc. Am. Proc.* **31**: 312-314.

Vachaud, G., Vauclin, M., and Wakil, M. 1972. A Study of the Uniqueness of the Soil Moisture Characteristic During Desorption by Vertical Drainage. *Soil Sci. Soc. Am. Proc.* **36**: 531-532.

Van Duijn, C.J., Molenaar, J. and Neef, M.J. 1995. The Effect of Capillary Forces on Immiscible Two-Phase Flow in Heterogeneous Porous Media. *Transp. Porous Media* **21** (1): 71-93.

Warren, J.E. and Root, P.J. 1963. The Behavior of Naturally Fractured Reservoirs. *SPE J.* **3** (3): 245-255; *Trans*., AIME, **228**. SPE-426-PA.

Yortsos, Y.C. 1991. A Theoretical Analysis of Vertical Flow Equilibrium. Paper SPE 22612 presented at the SPE Annual Technical Conference and Exhibition, Dallas, Texas, 6-9 October.

Yu, L., Evje, S., Kleppe, H., Karstad, T., Fjelde, I., and Skjaeveland, S.M. 2009. Spontaneous Imbibition of Seawater into Preferentially Oil-Wet Chalk Cores-Experiments and Simulations. *J. Pet. Sci. Eng.* **66** (3-4): 171-179.

Zanini, L., Novakowski, K.S., Lapcevic, P., Bickerton, G.S., Voralek, J., and Talbot, C. 2000. Ground Water Flow in a Fractured Carbonate Aquifer Inferred from Combined Hydrogeological and Geochemical Measurements. *Ground Water* **38** (3): 350-360.